GPCRs steer Gi and Gs selectivity via TM5-TM6 switches as revealed by structures of serotonin receptors

Huang, Sijie; Xu, Peiyu; Shen, Dan Dan; Simon, Icaro A.; Mao, Chunyou; Tan, Yangxia; Zhang, Huibing; Harpsøe, Kasper; Li, Huadong; Zhang, Yumu; You, Chongzhao; Yu, Xuekui; Jiang, Yi; Zhang, Yan; Gloriam, David E.; Xu, H. Eric

published in
Molecular cell
2022

DOI (link to publisher)
10.1016/j.molcel.2022.05.031

document version
Publisher's PDF, also known as Version of record

Molecular Cell

Article

GPCRs steer G_i and G_s selectivity via TM5-TM6 switches as revealed by structures of serotonin receptors

Graphical abstract

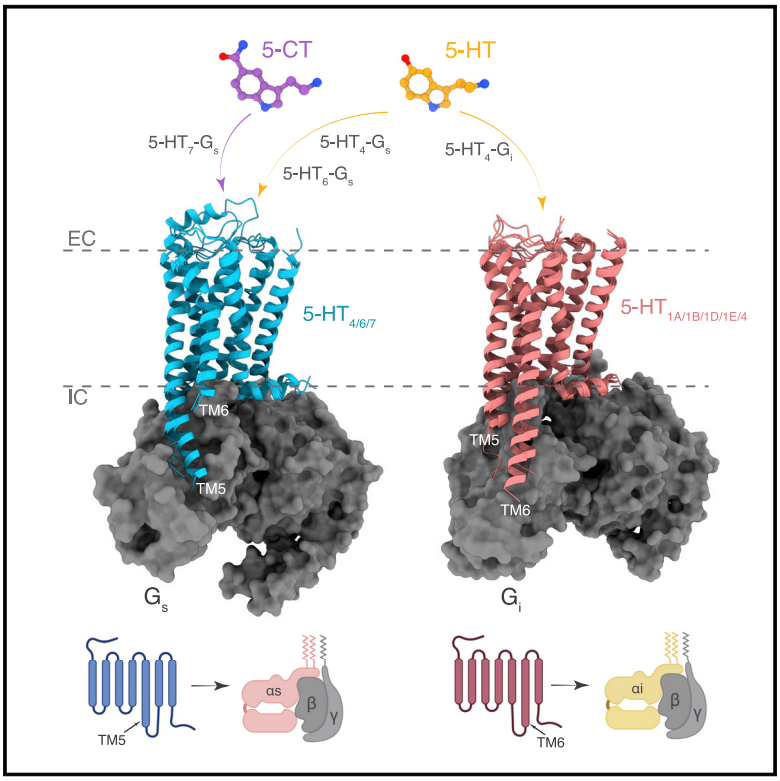

Highlights

- Cryo-EM structures of serotonin receptor 5-HT_4, 5-HT_6, and 5-HT_7 complexed with $G\alpha_s$
- Cryo-EM structure of serotonin receptor 5-HT_4 complexed with $G\alpha_i$
- The conserved binding mode of serotonin and the selective binding mode of 5-CT
- The TM5-TM6 switches are key to G_s and G_i selectivity for class A GPCRs

Authors

Sijie Huang, Peiyu Xu, Dan-Dan Shen, ..., Yan Zhang, David E. Gloriam, H. Eric Xu

Correspondence

zhang_yan@zju.edu.cn (Y.Z.), david.gloriam@sund.ku.dk (D.E.G.), eric.xu@simm.ac.cn (H.E.X.)

In brief

Huang et al. report four structures of the serotonin receptors 5-HT_4, 5-HT_6, and 5-HT_7 with G_s, and 5-HT_4 with G_{i1}. The structures reveal that transmembrane helices TM5 and TM6 alternate lengths as a macro-switch to determine receptor's selectivity for G_s and G_i, respectively.

Huang et al., 2022, Molecular Cell *82*, 2681–2695
July 21, 2022
https://doi.org/10.1016/j.molcel.2022.05.031

CellPress

Molecular Cell

CellPress

Article

GPCRs steer G_i and G_s selectivity via TM5-TM6 switches as revealed by structures of serotonin receptors

Sijie Huang,[1,2,3,12] Peiyu Xu,[1,2,12] Dan-Dan Shen,[4,5,6,12] Icaro A. Simon,[7,8,11,12] Chunyou Mao,[4,5,6] Yangxia Tan,[1,2,3] Huibing Zhang,[4,5,6] Kasper Harpsøe,[7] Huadong Li,[1,2,3] Yumu Zhang,[1,2,3] Chongzhao You,[1,2] Xuekui Yu,[1,9] Yi Jiang,[1,2] Yan Zhang,[4,5,6,10,*] David E. Gloriam,[7,13,*] and H. Eric Xu[1,2,3,13,14,*]

[1]The CAS Key Laboratory of Receptor Research, Shanghai Institute of Materia Medica, Chinese Academy of Sciences, Shanghai 201203, China

[2]University of Chinese Academy of Sciences, Beijing 100049, China

[3]School of Life Science and Technology, ShanghaiTech University, Shanghai 201210, China

[4]Department of Biophysics and Department of Pathology of Sir Run Run Shaw Hospital, Zhejiang University School of Medicine, Hangzhou 310058, China

[5]Liangzhu Laboratory, Zhejiang University Medical Center, Hangzhou 311121, China

[6]MOE Frontier Science Center for Brain Research and Brain-Machine Integration, Zhejiang University School of Medicine, Hangzhou, Zhejiang 310058, China

[7]Department of Drug Design and Pharmacology, University of Copenhagen, Universitetsparken 2, 2100 Copenhagen, Denmark

[8]SARomics Biostructures AB, Scheelevägen 2, 223 63 Lund, Sweden

[9]Cryo-Electron Microscopy Research Center, Shanghai Institute of Materia Medica, Chinese Academy of Sciences, Shanghai 201203, China

[10]Key Laboratory of Immunity and Inflammatory Diseases of Zhejiang Province, Hangzhou 310058, China

[11]Present address: Vrije Universiteit Amsterdam, Division of Medicinal Chemistry, Amsterdam Institute of Molecular and Life Sciences (AIMMS), Faculty of Science, De Boelelaan 1108, 1081 HZ Amsterdam, Netherlands

[12]These authors contributed equally

[13]Senior author

[14]Lead contact

*Correspondence: zhang_yan@zju.edu.cn (Y.Z.), david.gloriam@sund.ku.dk (D.E.G.), eric.xu@simm.ac.cn (H.E.X.)

https://doi.org/10.1016/j.molcel.2022.05.031

SUMMARY

Serotonin (or 5-hydroxytryptamine, 5-HT) is an important neurotransmitter that activates 12 different G protein-coupled receptors (GPCRs) through selective coupling of G_s, G_i, or G_q proteins. The structural basis for G protein subtype selectivity by these GPCRs remains elusive. Here, we report the structures of the serotonin receptors 5-HT_4, 5-HT_6, and 5-HT_7 with G_s, and 5-HT_4 with G_{i1}. The structures reveal that transmembrane helices TM5 and TM6 alternate lengths as a macro-switch to determine receptor's selectivity for G_s and G_i, respectively. We find that the macro-switch by the TM5-TM6 length is shared by class A GPCR-G protein structures. Furthermore, we discover specific residues within TM5 and TM6 that function as micro-switches to form specific interactions with G_s or G_i. Together, these results present a common mechanism of G_s versus G_i protein coupling selectivity or promiscuity by class A GPCRs and extend the basis of ligand recognition at serotonin receptors.

INTRODUCTION

The monoamine neurotransmitter serotonin (5-Hydroxytryptamine or 5-HT) regulates several central and peripheral physiological processes, such as cardiovascular and pulmonary functions, gastrointestinal motility, cognition, mood, appetite, and addiction (Berger et al., 2009; Sharp and Barnes, 2020). Serotonin exerts its biological functions through interaction with the 5-HT_3 ion channel and twelve G protein-coupled receptors (GPCRs), which are classified into six subfamilies 5-HT_1, 5-HT_2, 5-HT_4, 5-HT_5, 5-HT_6, and 5-HT_7 (Nichols and Nichols, 2008). These subfamilies differ in their primary transducer, 5-HT_1 and 5-HT_5 to $G_{i/o}$, 5-HT_2 to $G_{q/11}$, and 5-HT_4, 5-HT_6, and 5-HT_7 to G_s (Nichols and Nichols, 2008). Since G_s stimulates and $G_{i/o}$ inhibits the production of the same secondary messenger, cyclic AMP, these transducers lead to opposite cellular responses. The biological preference for one of these pathways is illustrated by the fact that 219 receptors couple to either G_s or $G_{i/o}$ families, but only one-fifth (44) of these couple to both (Avet et al., 2020). The structural basis underlying this remarkable difference in G protein coupling preference by different GPCRs remains poorly understood.

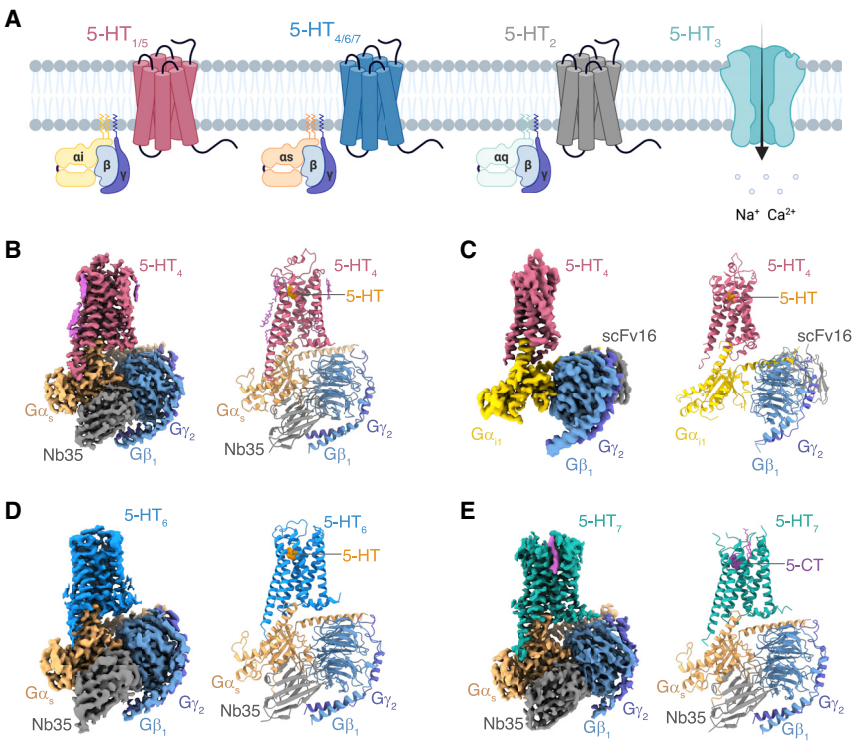

Figure 1. Cryo-EM structures of 5-HT$_4$, 5-HT$_6$, and 5-HT$_7$ signaling complexes

(A) Serotonin signaling through different subfamilies serotonin receptors.

(B–E) The cryo-EM density map (left) and model (right) of the serotonin bound complexes of 5-HT$_4$-G$_s$ (B), 5-HT$_4$-G$_i$ (C), 5-HT$_6$-G$_s$ (D), and the 5-CT bound complex of 5-HT$_7$-G$_s$ (E). See also Figures S1 and S2 and Table S1.

The 5-HT$_4$ receptor is a target for gastrointestinal motility treatments and its selective agonists have potential to improve pro-motility drugs' safety (Manabe et al., 2010). The 5-HT$_6$ receptor is expressed predominantly in the CNS and is considered a valuable target for cognitive enhancement (Mitchell and Neumaier, 2005). The 5-HT$_7$ receptor is involved in thermoregulation, circadian rhythm, learning, memory, and sleep, and is a potential target for the treatment of schizophrenia, depression, and alcohol abuse (Hauser et al., 2015; Nandam et al., 2007). These three serotonin receptor subtypes are known to have a high level of basal G$_s$-coupled activity and ligand-induced activation of ERK1/2 signaling (Liu et al., 2019b). Furthermore, these three receptors have only moderate sequence similarity to each other and to other serotonin receptor subtypes (Xu et al., 2021b). The structural basis of ligand recognition and G protein coupling by these three serotonin receptors remains unknown.

G$_{i/o}$- and G$_q$-bound structures have been reported for four and one serotonin receptor subtypes, respectively (Table S2), but no structure is available for the subtypes of G$_s$-coupled serotonin receptors. In this study, we present G$_s$ complex structures of all three serotonin receptors that primarily couple to G$_s$: 5-HT$_4$, 5-HT$_6$, and 5-HT$_7$. For 5-HT$_4$, we also present a structure complex with G$_{i1}$. Through structural comparison of these three G$_s$-coupled serotonin receptors to the G$_{i/o}$-coupled serotonin receptors, and to 19 additional G$_s$ and G$_{i/o}$-coupled class A receptor structures, we uncover a class-wide G protein selectivity mechanism through TM5 and TM6 switches. These findings advance the fundamental understanding of how serotonin receptors, the largest subfamily of class A GPCRs activated by the same endogenous ligand, create their wide diversity of cellular responses. Furthermore, these structural insights into ligand recognition provide the foundation for rational structure-based drug design at the 5-HT$_4$, 5-HT$_6$, and 5-HT$_7$ receptors, and for how to achieve ligand selectivity within the complex serotonergic system.

RESULTS

Cryo-EM structures of the 5-HT$_{4/6/7}$-G$_s$ complex and the 5-HT$_4$-G$_i$ complex

We used the wild-type full-length human 5-HT$_4$, 5-HT$_6$, and 5-HT$_7$ proteins for structural studies. To obtain receptor-G protein complexes, we co-expressed the receptors with a dominant-negative form of the human Gα_s or Gα_{i1} (Liang et al., 2018; Liu et al., 2016), the wild-type human Gβ_1 and human Gγ_2 in Sf9 or Hi5 insect cells. Serotonin was used to stabilize the complexes of 5-HT$_4$-G$_s$, 5-HT$_4$-G$_i$, and 5-HT$_6$-G$_s$, whereas a close serotonin analogue 5-Carboxamidotryptamine (5-CT) was used for the 5-HT$_7$-G$_s$ complex. To further stabilize the receptor-G protein complex, a nanobody, Nb35 (Rasmussen et al., 2011b) was added during 5-HT$_{4/6/7}$-G$_s$ complex formation and a single-chain antibody, scFv16 (Maeda et al., 2018), was co-expressed with the 5-HT$_4$-G$_i$ complex. The structures of the 5-HT$_4$-G$_s$, 5-HT$_4$-G$_i$, 5-HT$_6$-G$_s$, and 5-HT$_7$-G$_s$ complexes were determined at resolutions of 3.1 Å, 3.2 Å, 3.3 Å, and 3.2 Å, respectively (Figures S1 and S2). The EM density maps are sufficiently clear to define the position of the receptor, G protein heterotrimer, Nb35, scFv16, and the bound ligand in the receptor-G protein complexes (Figure 1; Figure S1 and S2). For all four complexes, the flexible receptor N termini, portions of the intracellular loop 3, and the Gα alpha-helical domain were not visible in the EM maps, as is also the case for most other GPCR-G protein complex structures. The seven transmembrane domain has a similar conformation across 5-HT$_4$, 5-HT$_6$, and 5-HT$_7$, which also have similar ligand binding pockets and binding modes (Figure 2). However, the extracellular loop 2 (ECL2), which forms a lid to the ligand binding pocket and exhibits distinct conformations in these receptors (Figure 1).

Serotonin binding modes in serotonin receptors

The serotonin binding pocket is lined by the transmembrane helices 3, 5, 6, and 7 (Figures 2A–2H). The strongest interaction is a

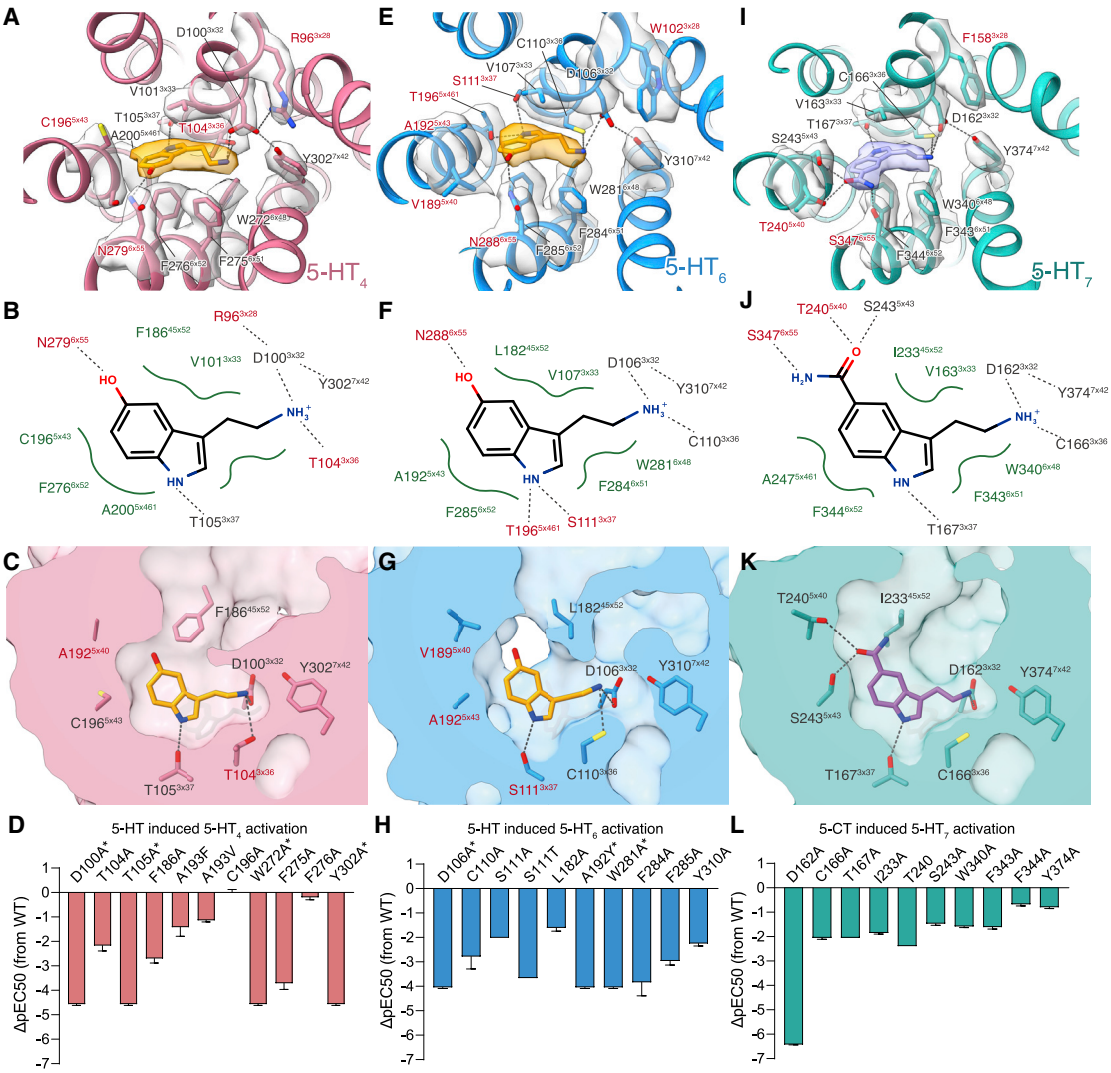

Figure 2. Molecular recognition of 5-HT$_4$, 5-HT$_6$, and 5-HT$_7$ receptors

(A–D) Conformation of the ligand-binding pocket in the serotonin-bound 5-HT$_4$-G$_s$ complex (A). Schematic representation of 5-HT-binding interactions. Hydrogen bonds are shown as black dashed lines. Hydrophobic contacts and amino acids are shown in green (B). Ligand-binding pocket shown as surface (C). 5-HT-induced β-arrestin2 recruitment assay for 5-HT$_4$ mutants using NanoBiT. All data are presented as mean values ± SEM with a minimum of four technical replicates and n = 3 biological replicates. See Figure S3 for dose response curves (D).

(E–H) Conformation of the ligand-binding pocket in the serotonin-bound 5-HT$_6$-G$_s$ complex (E). Schematic representation of 5-HT-binding interactions. Hydrogen bonds are shown as black dashed lines. Hydrophobic contacts and amino acids are shown in green (F). Ligand-binding pocket shown as surfaces (G). 5-HT-induced β-arrestin2 recruitment assay for 5-HT$_4$ mutants using NanoBiT. All data are presented as mean values ± SEM with a minimum of four technical replicates and n = 3 biological replicates. See Figure S3 for dose response curves (H).

(I–L) Conformation of the ligand-binding pocket in the 5-CT bound-5-HT$_7$-G$_s$ complex (I). Schematic representation of 5-HT-binding interactions. Hydrogen bonds are shown as black dashed lines. Hydrophobic contacts and amino acids are shown in green (J). Ligand-binding pocket shown as surfaces (K). Gs-cAMP accumulation results of 5-HT$_7$ mutants activated by 5-CT. All data are presented as mean values ± SEM with a minimum of four technical replicates and n = 3 biological replicates. See Figure S3 for dose response curves (L). * The activation of the mutant is too low to determine EC$_{50}$, which the corresponding ΔpEC$_{50}$ shown as the LogEC$_{50}$ value of the wild-type receptor. See also Figure S3.

salt-bridge between the ligand amine and receptor residue D^{3x32} (generic residue numbers from GPCRdb in superscript) (Isberg et al., 2015), a prototypical interaction for all bioamine GPCRs, including serotonin receptors (Vass et al., 2019). D^{3x32} is tethered by hydrogen bonds to Y^{7x42} in 5-HT$_4$, 5-HT$_6$, and 5-HT$_7$ and additionally to R^{3x28} in 5-HT$_4$. Mutations of any of these residues decrease serotonin potency (Figure 2). In addition, T^{3x36} and T^{3x37} in the 5-HT$_4$ receptor and S^{3x37} in the 5-HT$_6$ receptor form direct hydrogen bonds to serotonin (Figures 2B and 2F). Hydrophobic residues are also critical for serotonin binding. In 5-HT$_4$, V101^{3x33}, F186^{45x52}, C196^{5x43}, A200^{5x461}, W272^{6x48}, F275^{6x51}, and F276^{6x52} form hydrophobic contacts with the

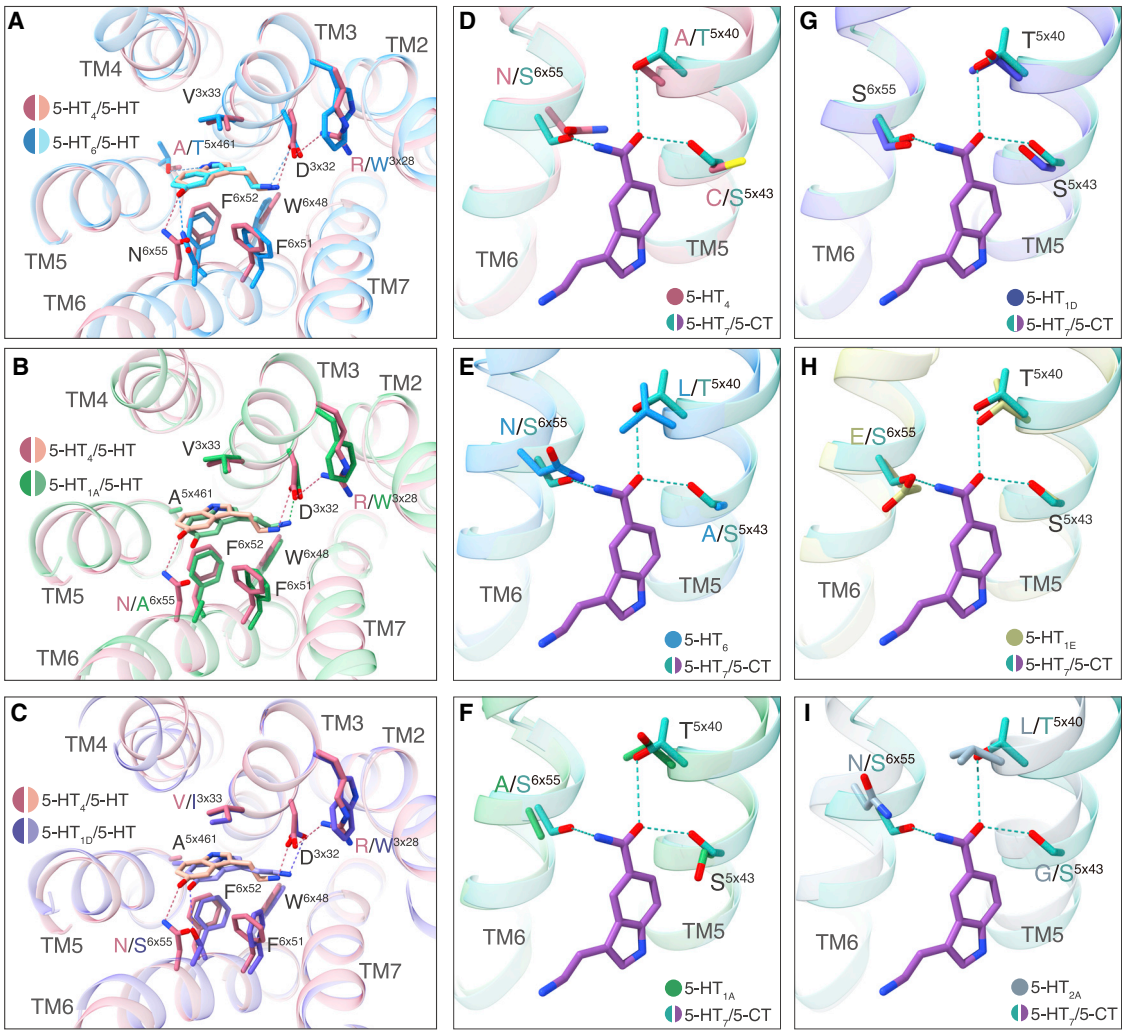

Figure 3. Comparisons of serotonin binding poses and 5-CT selectivity in different serotonin receptors

(A–C) Comparison of ligand recognition between 5-HT_4- and 5-HT_6-binding serotonin (A). Comparison of ligand recognition between 5-HT_4 and 5-HT_{1A} binding serotonin (B). Comparison of ligand recognition between 5-HT_4 and 5-HT_{1D} binding serotonin (C).

(D–I) Comparison of residues in 5-HT_7 recognizing 5-CT with the corresponding residues among other serotonin receptors. PDB code: 5-HT_{1A}, 7E2Y; 5-HT_{1D}, 7E32; 5-HT_{1E}, 7E33; 5-HT_{2A}, 6WHA. See also Figures S3 and S4.

indole scaffold of serotonin (Figures 2A and 2B). Correspondingly, in 5-HT_6, $V107^{3x33}$, $L182^{45x52}$, $A192^{5x43}$, $W281^{6x48}$, $F284^{6x51}$, $F285^{6x52}$ form hydrophobic contacts with serotonin (Figures 2E and 2F). The stronger aromatic π-π interaction with F^{6x51} than F^{6x52} is supported by mutagenesis data and ligand affinity measurements with alanine mutation, especially in the 5-HT_6 receptor (Figures 2D, 2H, and S3).

Comparison of our 5-HT_4, 5-HT_6, and previous (5-HT_{1A} and 5-HT_{1D}) serotonin-bound structures (Xu et al., 2021b) shows a conserved amine-D^{3x32} salt-bridge and hydrophobic contacts of the indole with the TM3 residue V/I^{3x33} and TM6 residues F^{6x51} and F^{6x52} (Figures 3A–3C). However, the 5-$HT_{4/6/1A/1D}$ ligand-binding pockets comprise residues with unique features at positions 3x28, 5x461, and 6x55 (Figures 3A–3C). At position 3x28, 5-HT_4 has a unique residue $R96^{3x28}$, which is part of a hydrogen-bonding network formed by the key residues, $R96^{3x28}$ and Y^{7x42} that tethers D^{3x32} in position to form the amine saltbridge (Figures 2A, 3A–3C). Notably, all other serotonin receptors instead have a hydrophobic residue W or F in position 3x28 (Figure S4A). F^{3x28} in 5-HT_{1A} contacts the antipsychotic drug aripiprazole (Xu et al., 2021b) suggesting that the residue in position 3x28 plays a key role in drug recognition and selectivity. At position 5x461, 5-HT_6 has a unique residue T^{5x461} forming a hydrogen bond with the serotonin indole nitrogen that cannot be formed by the corresponding A^{5x461} in 5-$HT_{4/1A/1D}$ (Figures 2E, 3A–3C). Moreover, at position 6x55, 5-HT_{1A} has an Ala and therefore lacks the polar group to form the hydrogen bond found in the 5-HT_4, 5-HT_6 (Asn), and 5-HT_{1D} (Ser) receptors (Figures 3A–3C and S4). Together, these unique binding site residues present alternative physicochemical properties and opportunities for drug design seeking to optimize receptor selectivity.

Selective binding mode of 5-CT in the 5-HT$_7$ receptor

5-CT exhibits higher affinities for 5-HT$_7$, 5-HT$_{1A}$, 5-HT$_{1B}$, and 5-HT$_{1D}$ than for other serotonin receptors (Pauwels, 2000; Yamada et al., 1998). In the 5-HT$_7$ structure, 5-CT resembles serotonin in receptor binding (Figures 2I–2K), with the same canonical amine-D^{3x32} salt-bridge, indole-F^{6x51} hydrophobic interaction, and indole-T^{3x37} hydrogen bond (Figures 2I and 2J). However, the distinct 5-amide-subtituent of 5-CT forms three additional hydrogen bonds with T^{5x40}, S^{5x43}, and S^{6x55} (Figures 2I and 2J). T^{5x40} and S^{5x43} are only conserved in the 5-HT$_7$ and 5-HT$_1$ subfamilies (Figure S4A) and therefore contribute to selectivity. Importantly, position 6x55 holds a small side chain (Ser or Ala) in 5-HT$_7$, 5-HT$_{1A}$, 5-HT$_{1B}$, and 5-HT$_{1D}$, but a bulkier side chain (Asn or Glu) in other serotonin receptors (Figures 3D–3I and S4A). Comparison of the 5-HT$_7$ and 5-HT$_{1E}$ structures shows that the bulkier E^{6x55} in 5-HT$_{1E}$ would clash with the amide group of 5-CT in a similar binding pose, thus reducing the binding affinity of 5-CT to 5-HT$_{1E}$ (Figure 3H). The importance of 6x55 for ligand selectivity agrees with our previous findings for dopamine and serotonin receptors (Xu et al., 2021a, 2021b) and further stress the role on 6x55 in the ligand binding selectivity of bioamine receptors.

Common and unique features in the G$_s$ binding pockets of 5-HT$_{4/6/7}$

The 5-HT$_{4/6/7}$-G$_s$ complexes are mainly stabilized by electrostatic interactions between Gα_s and the receptors. The Gα C-terminal α5 helix and Ras domain feature negative charges complemented by positive charges on the receptor TM5 (Figures 4A–4C). Similar electrostatic interactions are present in multiple GPCR-G protein structure complexes (Xu et al., 2021a). This suggests that the electrostatic interactions are a critical driving force for the coupling of G proteins to receptors. Comparison of the G$_s$-coupling interfaces of 5-HT$_4$, 5-HT$_6$, and 5-HT$_7$ reveals several distinct features (Figure 4). Firstly, the receptor ICL2 has strong interactions with the G$_s$ α5-αN domain in all receptors but their conformations differ from each other (Figures 4D–4F). Here, residue N^{34x55} and V^{34x52} in 5-HT$_4$ forms polar and hydrophobic contacts to Q35 and V217 in Gα_s, respectively (Figure 4D), but the corresponding residue in 5-HT$_6$ and 5-HT$_7$ is R^{34x52} and T^{34x52} that cannot provide the correspondingly interactions (Figures 4E and 4F). Secondly, in the 5-HT$_4$-G$_s$ structure, the cytoplasmic end of TM5 forms a longer helix bent towards TM6, while in the 5-HT$_6$- and 5-HT$_7$-G$_s$ structures, it instead forms a shorter helix linked with a loop (Figures 4G–4I). To accommodate the different conformations of TM5, the Gα_s-Ras domain of these three complexes is shifted relative to each other, which is most obvious for the 5-HT$_4$-G$_s$ complex (Figure 4J). Although the cytoplasmic end of TM5 displays different conformations in the three structures, the extension of TM5 and the additional interface between TM5 and Gα_s is a common feature among the G$_s$-coupled GPCR complex structures (Figure S5B), such as β_2-G$_s$ (Rasmussen et al., 2011b), D$_1$-G$_s$ (Zhuang et al., 2021), and GPR52-G$_s$ (Lin et al., 2020), suggesting that the TM5-Gα_s contacts are broadly involved in G$_s$ coupling.

Dual 5-HT$_4$ complexes reveal the basis of G$_s$ versus G$_i$ selectivity

Previous reports showed that 5-HT$_4$ can both couple to G$_s$ family (G$_s$ and G$_{olf}$) and G$_i$ family (G$_{i1}$, G$_{i3}$, G$_o$, and G$_z$) with preference for G$_s$ over G$_i$ (Inoue et al., 2019a; Pindon et al., 2002). Our G$_s$- and G$_{i1}$-coupled 5-HT$_4$ complexes uniquely provide structural insights into differential coupling of the same class A receptor to two G proteins with opposite functions i.e., stimulation or inhibition of cAMP production, respectively. We find that the overall structures of 5-HT$_4$ bound to G$_s$- and G$_i$ are very similar, with a root-mean-square deviation (RMSD) of 0.48 Å for the receptor Cα atoms (Figure 5A). Their orthosteric binding pockets are virtually identical (all-atom RMSD 0.38 Å for residues within 6 Å of serotonin). This indicates that, in the case of serotonin, the G protein selectivity arises intrinsically from the receptor, rather than through a serotonin-induced mechanism. This finding is corroborated by the common binding mode of serotonin in the G$_s$-coupled structures reported here and structures of the G$_i$-coupled 5-HT$_{1A}$ and 5-HT$_{1D}$ (Xu et al., 2021b). However, a striking difference is observed in the intracellular end of TM5, which is extended by 12 residues (3 helical turns) in the G$_s$-coupled compared to G$_{i1}$-coupled 5-HT$_4$ receptor (Figures 5A–5C). Due to this extension, the C-terminal α5 of the Gα_s subunit binds in a 20.2° tilted conformation relative to that α5 in G$_{i1}$ (Figures 5D–5F). This tilt is associated with a relocation of the Gα_s-α5 away from TM5 and towards TM3, while the top of α5 buried in the receptor core is closer to TM6. This causes the TM6 of the G$_s$ complex to move 3.0 Å more outwards compared to the G$_i$ complex (Figure 5C) in concordance with cross-receptor comparisons published with the first G$_{i/o}$-coupled structures (Capper and Wacker, 2018; Kang et al., 2018b). Interestingly, the insertion angle of the G protein α5 axis relative to the membrane plane is little affected being 47.1° for the G$_{i1}$- and 45.6° for the G$_s$-coupled 5-HT$_4$. The mentioned tilt of α5 is transmitted to the Gα subunit and to the whole G protein (Figure 5F), making the interface of G$_s$-coupled 5-HT$_4$ more than double as large as the G$_i$-coupled 5-HT$_4$ interface (1,667 Å^2 compared to 773 Å^2). Together, these structural insights demonstrate how 5-HT$_4$, as a typical class A GPCR, can shift conformation to present distinct binding pockets for G$_s$ and G$_{i1}$.

Alternating long TM5 and TM6 helices switch G$_s$ and G$_{i/o}$ selectivity

Our G$_s$-coupled 5-HT$_{4/6/7}$ and G$_{i1}$-coupled 5-HT$_4$ structures and the previous 5-HT$_1$-G$_{i/o}$ (Garcia-Nafria et al., 2018b; Xu et al., 2021b) structures together give an unprecedented basis to investigate GPCR-G protein coupling selectivity for a receptor family that shares endogenous ligand and high sequence homology (Figures 6A and 6B). Therefore, we sought to investigate if the G$_s$ versus G$_{i1}$ selectivity mechanism observed for 5-HT$_4$ is conserved in other serotonin receptors. We find that G$_s$-coupled 5-HT$_{4/6/7}$ receptors have a cytosolic TM5 that is on average 5.7 residues longer (Figures 6A and 6B) and a TM6 that is 7.5 residues shorter compared to the G$_{i/o}$-coupled 5-HT$_{1/4}$ receptors (Figure 6, Table S3). Remarkably, the differential length of these two helices amounts to 13.2 ± 4.3 residues across the G$_s$ and G$_{i/o}$-coupled serotonin receptors ($p = 0.022$) (Figure S5A). The extension of TM5 of G$_s$-coupled receptors provides unique interactions that are not seen in the G$_i$ complexes. This difference is mainly attributed to the distinct feature of the Ras-domain between G$_s$ and G$_{i/o}$. The Ras-domain is 13 residues longer in G$_s$ than in G$_{i/o}$ and enlarging a loop oriented towards the plasma membrane (Figures 5E and 6A). This loop together with the α4

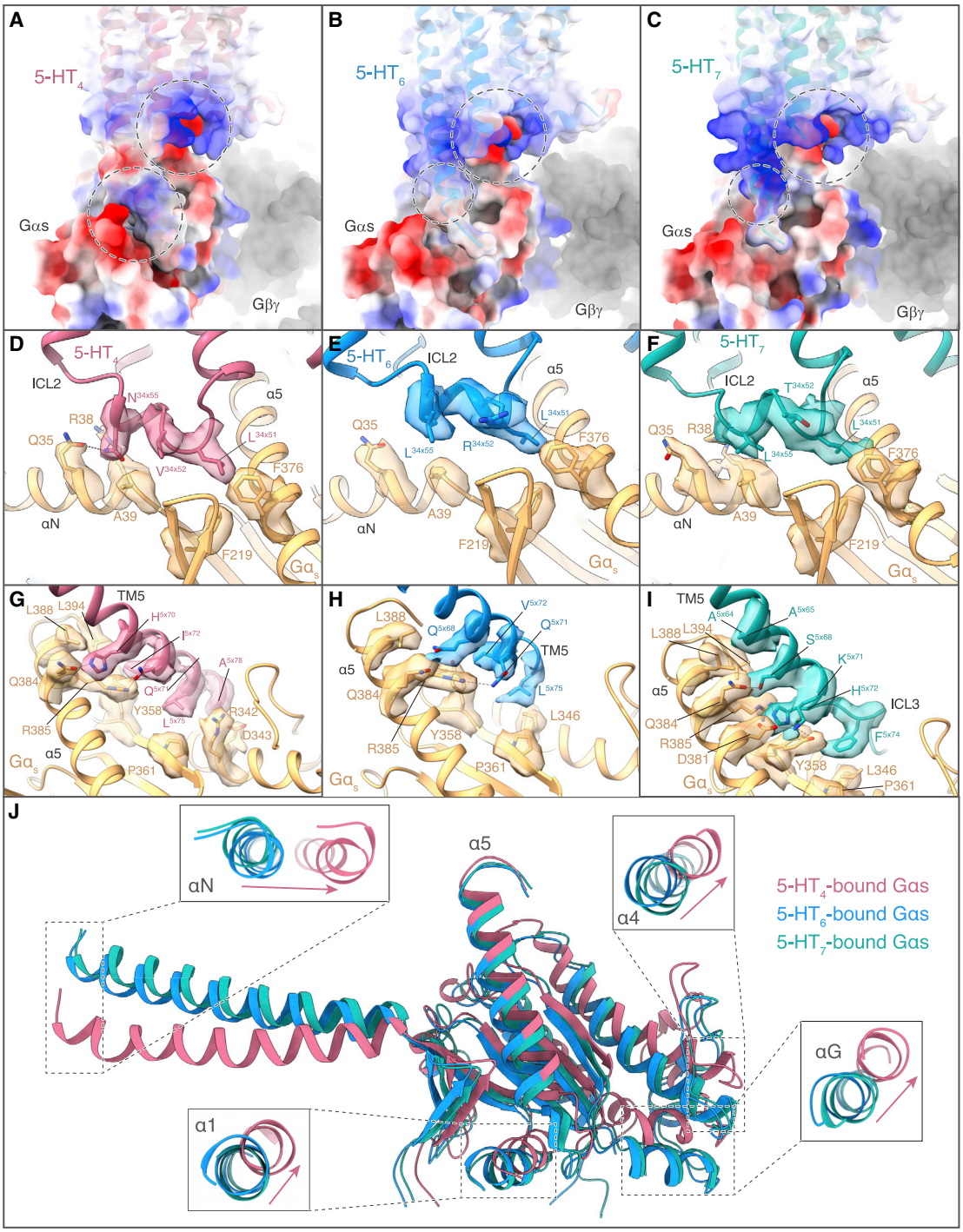

Figure 4. G protein coupling of 5-HT$_4$, 5-HT$_6$, and 5-HT$_7$ receptors

(A, D, G) Interactions between 5-HT$_4$ and Gα_s subunits. Electronic interaction between the 5-HT$_4$ and Gαs protein binding interface (A). Residues model of interaction is shown in (D) and (G).

(B, E, H) Interactions between 5-HT$_6$ and Gα_s subunits. Electronic interaction between the 5-HT$_6$ and Gαs protein binding interface (B). Residues model of interaction is shown in (E) and (H).

(C, F, I) Interactions between 5-HT$_7$ and Gα_s subunits. Electronic interaction between the 5-HT$_7$ and Gαs protein binding interface (C). Residues model of interaction is shown in (F) and (I).

(J) Comparison of the Gα conformation among the structures of G$_s$-coupled 5-HT receptors. See also Figures S4 and S6.

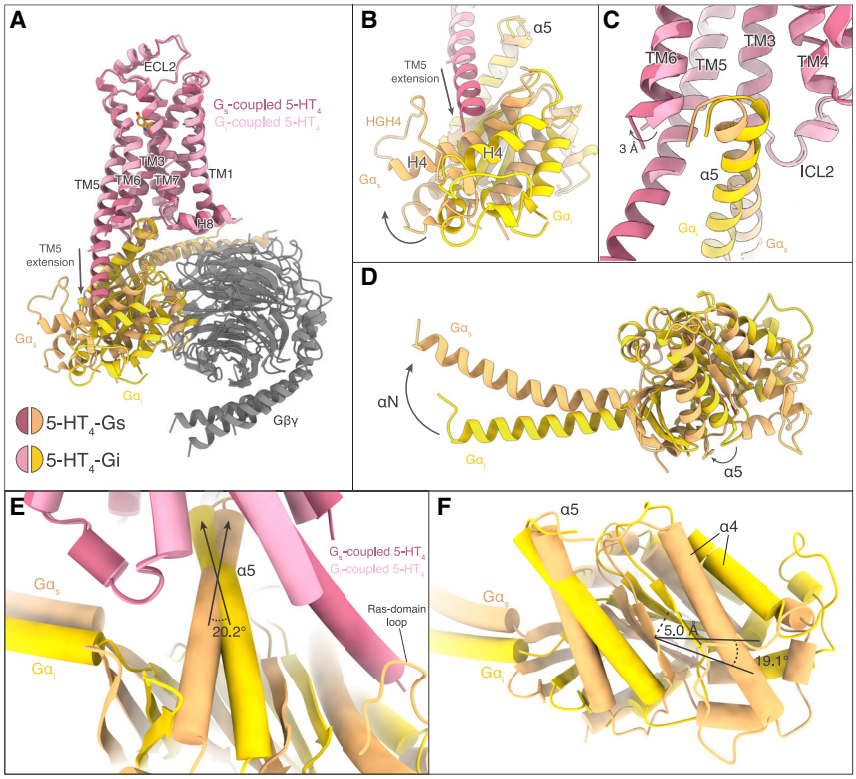

Figure 5. Comparison of the 5-HT$_4$-G$_s$ complex with the 5-HT$_4$-G$_i$ complex

(A) Structural alignment of the 5-HT$_4$-G$_s$ and 5-HT$_4$-G$_i$ complexes.

(B) Superposition of TM5 and the Gα$_s$ and Gα$_i$ subunits.

(C) Differences in the α5 helix of Gα$_s$ and Gα$_i$ subunits.

(D) Differences in the αN helix of Gα$_s$ and Gα$_i$ subunits.

(E) The relative tilt/rotation angle between the C-terminal α5 helices in the G$_s$- and G$_i$-coupled complexes of 5-HT$_4$.

(F) Differences in angle and position of the whole Gα-subunit (except the N terminus helix) between the G$_s$- and G$_{i/o}$-coupled 5-HT$_4$. See also Figures S4 and S5 and Table S4.

helix of Gα$_s$ form close contacts with the cytoplasmic TM5 not present in the G$_i$ complexes (Figures 5E, 5F, and 6A). In addition, Nb35-bound or no-Nb35-bound 5-HT$_4$-G$_s$ complex shares the common extended TM5 structure (Figure S5H), which is different from the G$_i$-coupled 5-HT$_4$-G$_i$ complex. This suggests the TM5 extension is not affected by the antibody. Thus, the relative lengths of TM5 and TM6 in serotonin receptors serves as a "macro-switch" to determine the G$_s$ or G$_{i/o}$ coupling selectivity.

We next investigated if the macro-switch by the TM5-TM6 length is conserved across class A GPCRs by expanding our analysis to 27 G$_s$- or G$_{i/o}$-coupled structures (all distinct GPCR-G protein pairs, except chimeric G proteins in complex with the 5-HT$_{2A}$ and orexin-2 receptors; Table S2) (Draper-Joyce et al., 2018a; Garcia-Nafria et al., 2018a; Hong et al., 2021; Hua et al., 2020; Israeli et al., 2021; Kato et al., 2019; Kim et al., 2020; Koehl et al., 2018a; Liu et al., 2020; Maeda et al., 2019; Nojima et al., 2021; Su et al., 2020; Wasilko et al., 2020; Xia et al., 2021; Xing et al., 2020; Yang et al., 2020; Yuan et al., 2020; Zhuang et al., 2020; Rasmussen et al., 2011b; Zhuang et al., 2021; Lin et al., 2020; Xu et al., 2021b; Garcia-Nafria et al., 2018b; Draper-Joyce et al., 2018b; Xu et al., 2021a). When comparing G$_s$- to G$_{i/o}$-coupled receptors, we find that TM5 is 5.6 ± 1.5 residues longer ($p = 0.0012$) (Figure S5C; Table S3), TM6 is 2.6 ± 1.6 residues shorter ($p = 0.114$) (Figure S5D), and the differential TM5-TM6 length is 8.2 ± 2.1 residues, i.e., ~2 helical turns ($p = 6.4\times10^{-4}$) (Figure S5E). Although the individual helix length difference is only significant for TM5, combining this helix with TM6 into the "TM5-TM6 length switch" increases the length difference and significance. Thus, the macro-switch by the TM5-TM6 length is conserved across class A (Figure S5B). To test if this relative length difference may apply also to other class A receptors for which a structure is not yet available, we predicted the helical content of a stretch of 40 residues between positions 5x50 and 6x50 using the sequence-based JPred Protein Secondary Structure Prediction Server (Cuff and Barton, 2000; Drozdetskiy et al., 2015) (Figure S5F). This reproduced the statistically significant ($p = 1.8\times10^{-4}$) TM5-TM6 length difference between G$_s$ and G$_{i/o}$ coupled receptors, with an average number of residues that is even larger than the observed difference seen in the structures (11 ± 2.5 compared to 8.2 ± 2.1 residues; Figures S5E and S5F).

The above analysis suggests that TM5-TM6 is the determinant of the selectivity of G$_s$ protein for 5-HT$_{4/6/7}$ and G$_{i/o}$ protein for 5-HT$_{1A}$. To explore this hypothesis of G-protein preference for serotonin receptors, we performed two set of experiments to test the hypothesis that the length of TM5 and TM6 is the key factor for GPCRs to discriminate Gs and Gi (Figures 6G–6L).

The first set of experiments are to introduce helix-breaking mutations at the end of TM6 into 5-HT$_{1A}$, and TM5 in 5-HT$_{4/7}$, plus extending TM5 in 5-HT$_{1A}$, extending TM6 in 5-HT$_{4/7}$. Such mutations affect the G$_s$-coupled ability of 5-HT$_{4/7}$ (Figures 6G and 6H) and can convert 5-HT$_{1A}$ into a G$_s$-coupled receptor (Figure 6I). These results further support that the length of TM5 and TM6 are the key for G protein selectivity. The second set of experiments are to swap the TM5-TM6 region of the G$_i$-couple 5-HT$_{1A}$ with that of Gs coupled receptors 5-HT$_4$ and 5-HT$_7$. We replaced the intracellular half of TM5, TM6, and ICL3 (P$^{5.50}$ to P$^{6.50}$) of 5-HT$_{1A}$ receptor with 5-HT$_{4/7}$ receptors and tested their 5-HT induced cAMP accumulation. Our results show that the chimeric receptor 5-HT$_{1A}$ (5-HT$_4$_P$^{5.50}$-P$^{6.50}$) displays a similar function with the wild-type 5-HT$_4$, which has high constitutive activation and is hardly regulated by the ligand (Figure 6J), consistent with our previous report (Liu et al., 2019a). Similarly, 5-HT$_{1A}$ (5-HT$_7$_P$^{5.50}$-P$^{6.50}$) displays a similar function with the wild-type 5-HT$_7$, stimulating the accumulation of cAMP induced by the agonist (Figure 6K). If the

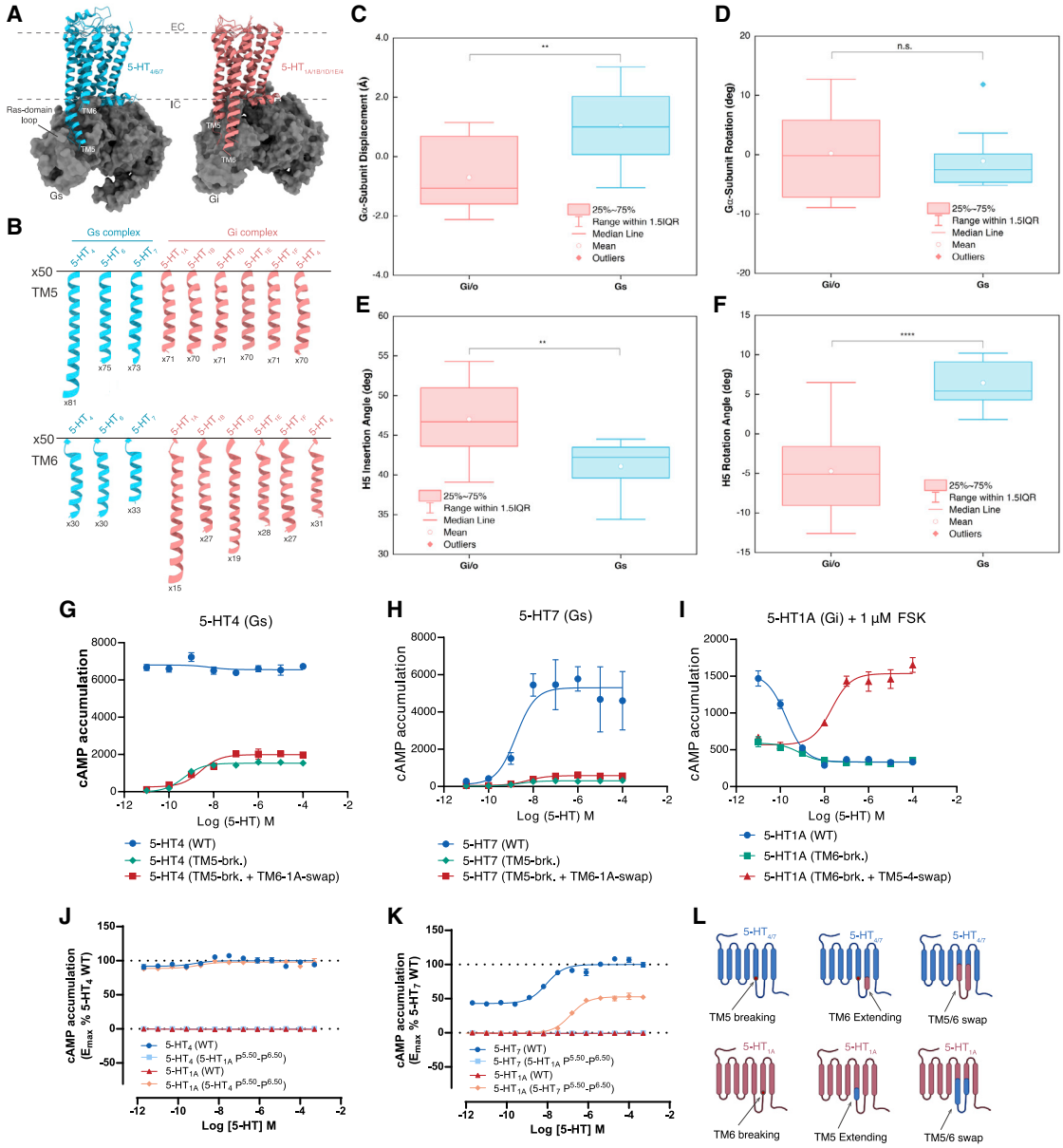

Figure 6. Receptor TM5 and TM6 lengths determine differential insertion angles and tilts of Gα helix 5

(A) Superposition of G_s- (left) and G_i-coupled (right) serotonin receptor structures.

(B) Length comparison of transmembrane helices 5 and 6 (TM5 and TM6) across serotonin receptor structures.

(C–F) Receptor TM5 and TM6 lengths macro-switch determine insertion angles and tilts of Gα helix 5. For the whole set of 28 class A G_s- or $G_{i/o}$-coupled receptor structures, (C) there is a significant difference in positioning of the G_α subunit ($p = 0.0010$) but (D) no significant difference ($p = 0.625$) in the rotation angle of the G_α subunit across these two G protein families. (E) The relatively longer TM5 and shorter TM6 in G_s-coupled receptors make the G_s C-terminal α5 bind in average 5.9° more parallel to the membrane than in $G_{i/o}$ ($p = 0.0012$) while (F) promoting a 11.2° rotation of α5 towards TM3 and the ICL2 in the comparison with the $G_{i/o}$-coupled receptor complexes ($p = 5.09 \times 10^{-7}$).

(G–H) The activation of 5-HT_4 (G) and 5-HT_7 (H) affected by TM5 helix breaking or plus extending TM6 by 5-HT_{1A} sequence.

(I) The activation of 5-HT_{1A} affected by TM6 helix breaking or plus extending TM5 by 5-HT_4 sequence.

(J–K) The activation of chimeric receptors, exchanges $P^{5.50}$ to $P^{6.50}$ between 5-HT_{1A} and 5-HT_4 (J) and 5-HT_{1A} and 5-HT_7 (K).

(L) The activation of 5-HT_6 affected by the swap of receptor-G protein interface between G_s and G_i. See also Figures S5 and S7 and Tables S2 and S3.

intracellular half of TM5/6 and the ICL3 of 5-HT_4 and 5-HT_7 were replaced with that of 5-HT_{1A}, their ability to stimulate the accumulation of cAMP was almost lost, resembling the WT 5-HT_{1A} (Figures 6J and 6K). This swap makes 5-HT_{1A} from a G_i-coupled receptor to a G_s-coupled receptors, supporting that the TM5-TM6 regions are key for G protein selectivity.

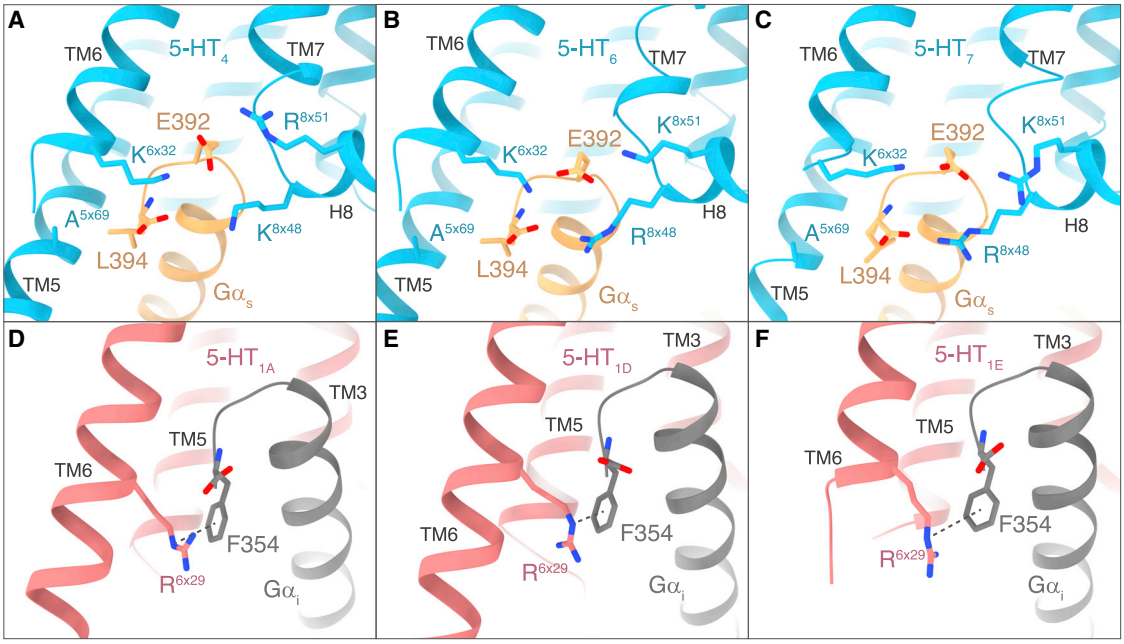

Figure 7. Differences between G_s- and G_i-coupled serotonin receptors

(A–C) Receptor (5-HT_4, A; 5-HT_6, B; 5-HT_7, C) interactions with the α5 terminus of $G\alpha_s$ subunit.

(D–F) Receptor (5-HT_{1A}, D; 5-HT_{1D}, E; 5-HT_{1E}, F) interactions with the α5 terminus of $G\alpha_i$ subunit. See also Figures S5 and S7 and Table S4.

G_s and $G_{i/o}$ adapt to receptors through mutual mechanisms

We next investigated if the structural differences in the receptors are reflected by specific and distinct binding of the G_s and $G_{i/o}$ proteins, as seen for 5-HT_4. Comparison of serotonin receptor structure complexes shows that G_s is buried deeper (2.0 ± 0.7 Å) into the receptor core than $G_{i/o}$ ($p < 0.03$). The same trend is also observed for the 28 class A G_s and $G_{i/o}$ complexes, which display an increased insertion of 1.7 ± 0.5 Å ($p < 0.002$) of the G_s versus $G_{i/o}$ α-subunit into the receptor core (Figure 6C), although no significant difference is seen for the rotation of the Gα-subunit relative to the receptor core across the two G protein families (Figure 6D).

Given that the C-terminal α5 helix of G protein forms most receptor contacts and has direct contacts with TM5 and TM6, we specifically investigated its movement. A significant difference ($p = 0.0012$) in the insertion angle into the receptor transmembrane bundle was observed for the α5 helix of G_s and $G_{i/o}$. This angle is smaller in G_s- than in $G_{i/o}$-coupled structures to accommodate the long receptor TM5 (41.1 ± 3.4° versus 47.0 ± 4.7°, respectively, Figure 6E). Furthermore, when analyzing the tilt of the G protein α5 helix within the receptor core we found an even larger difference (11.2 ± 1.7°, $p = 5.1 \times 10^{-7}$, Figure 6F). The long TM5 and short TM6 of G_s-coupled receptors is associated with a rotation of the lower part of the α5 helix away from TM5 towards TM3 and ICL2, while the short TM6 also allows the C-terminal end of the α5 helix to be closer to TM6. The opposite pattern is seen for the $G_{i/o}$-coupled class A receptors for which the short TM5 and long TM6 are instead associated with a rotation of the α5 helix of $G_{i/o}$ away from TM3 and ICL2. Together, this demonstrates that G proteins adapt to their receptors by engaging in mutual recognition mechanisms that can be seen even in closely related receptors and are shared by many class A GPCRs.

Receptor residue "micro-switches" for G_s and $G_{i/o}$ span TM3, ICL2, TM5, and TM6

We next investigated the residue level determinants that mediate G_s and $G_{i/o}$ coupling selectivity. To this end, we constructed residue-to-residue interaction matrices, which show the consensus contacts of G_s- or $G_{i/o}$-bound serotonin and class A receptor structures, respectively (Figure S6). Residue "micro-switches" contributing to coupling selectivity were defined by contacts with at least 33% higher frequency in G_s or $G_{i/o}$ complexes. This revealed that even the closely related serotonin receptor subtypes contain 14 G_s- or $G_{i/o}$-specific protein interactions between 10 receptor residues and 12 Gα-subunit residues (Figure S4B). Furthermore, when extending this analysis to 27 class A receptors, we uncovered in total 25 G_s- or $G_{i/o}$-specific protein interactions between 15 receptor residues and 17 Gα-subunit residues (Figure S4C).

The receptor residues that contact the Gα-subunit span across TM3, ICL2, TM5, and TM6. Specifically, TM5 residues, including 5x68, 5x71, and 5x72 in the cytosolic end of TM5 form unique contacts to different portions of the G_s C-terminus. Position 5x72, in particular, which is often not present in $G_{i/o}$-coupled complexes, form distinct contacts to the C-terminal residues $L394^{\alpha5.26}$, $R385^{\alpha5.17}$, and $Y358^{\alpha4.s6.20}$, which are unique for G_s, (common G_α residue numbers from (Flock et al., 2015) in superscript, (Isberg et al., 2015), Figure S4C). These interactions are often absent in $G_{i/o}$-bound receptor complexes (Figure S4C), instead the distinct $G\alpha_i$ residue $F/Y354^{\alpha5.26}$ forms a cation-pi interaction with R/K^{6x29} on TM6 of G_i-coupled receptors (Figure 7). The G_s-specific

residue E392$^{\alpha5.24}$ also mediates contacts with G_s-coupled receptor residues in TM6 and H8 (6x32, 6x36, 8x48, and 8x51) to form an extensive network of hydrogen bonds and salt bridges (Figure 7). E392$^{\alpha5.24}$ and its preceding residue Y391$^{\alpha5.23}$ in G_s are bulkier than the corresponding residues in $G_{i/o}$ (G352$^{\alpha5.24}$ and C351$^{\alpha5.23}$, respectively), which leads to the tilting of $G\alpha_s$ $\alpha5$ helix towards TM3 and ICL2 to accommodate the long TM5 in G_s-coupled receptors (Figure 7).

The tilt of the G_s $\alpha5$ towards TM3 and the ICL2 is also reflected in the unique set of interactions of Gs with TM3 and ICL2 at positions 3x54, 3x55, 3x58, 34x51, and 34x54. These interactions constitute an anchoring hub, forming 11 of the 21 interactions unique to G_s proteins. The movement of G_s-$\alpha5$ towards TM3 and ICL2 creates a hydrophobic cavity between the receptor and G protein in which the ICL2 residue 34x51 is buried (Figures S7B and S7C). This hydrophobic cavity is large enough to accommodate bulky ICL2 residues in other Gs-coupled receptors, such as F^{34x51} in the β_2-adrenoceptor (Du et al., 2019; Rasmussen et al., 2011b) and D_1 (Zhuang et al., 2021). Conversely, the 11.2° shift of the $G_{i/o}$ $\alpha5$ helix toward the centre of the 7TM bundle (Figures 5E and 5F) prevents the formation of this hydrophobic cavity and blocks its interactions with ICL2. Together these specific residue-G protein interactions define "micro-switches" across the cytosolic interface of the receptor for specific coupling of G_s and $G_{i/o}$.

Sequence signatures expand the G_s versus $G_{i/o}$ selectivity residue micro-switches

To investigate G_s versus $G_{i/o}$ binding determinants and selectivity residue micro-switches for a larger number of receptors including those that lack G protein-bound structural templates, we performed a comparative sequence analysis using GPCRdb's sequence signature tool (Kooistra et al., 2021). This analysis encompassed 7 of the structure-based microswitches and 12 additional residue positions in cytosolic TM5 and TM6 that interact with G proteins in structure complexes with at least two different GPCRs. This uncovered consensus amino acids and properties in G_s- and $G_{i/o}$-activating receptors, as well as a sequence signature with distinctly conserved properties for only one of these G protein families (Table S5). We find that the average conservation of a residue property is substantially higher than for a specific amino acid for both G_s-coupled (TM5: 66% versus 32% and TM6: 71% versus 32%) and the $G_{i/o}$-coupled (TM5: 75% versus 39% and TM6: 69% versus 34%) receptors. The conservation of residue properties in two-thirds to three-quarters of receptors suggests that these constitute binding determinant of the G_s and $G_{i/o}$ families, respectively.

To uncover sequence-based selectivity residue micro-switches for G_s- versus $G_{i/o}$-activation, we identified a sequence signature consisting of properties that are distinctly conserved for only one of these G protein families ("Sequence signature" box in Table S5). For G_s-coupled receptors, the most distinctive property (41% more conserved than in $G_{i/o}$-coupled receptors) is a hydrophobic aromatic residue in position 5x65. The hydrophobic aromatic signature property recurs for four additional residue positions distinct for G_s (5x69 and 5x72) or $G_{i/o}$ (5x61 and 5x66). For $G_{i/o}$-coupled receptors, the two most distinctive (34% and 29%) residues positions, 5x73 and 5x71 contain a gap that denotes non-helical structure and are located at and close to the cytosolic helix end. Furthermore, three out of four residues closest to the cytosolic end of TM6 also contain a gap. This is consistent with our helix switch model. Other signature properties in TM6 span mainly small hydrogen-bonding or aliphatic-hydrophobic properties. This shows that several sequence-based selectivity microswitches contribute to the TM5 and TM6 helix macro-switches, whereas other microswitches may form specific molecular interactions with complementary G protein residues.

Rare dual G_s- and $G_{i/o}$-coupling receptors combine conserved and specific properties

GPCRs display an inverse correlation for the activation of the G_s and $G_{i/o}$ families (Hauser et al., 2022) and only 9 class A receptors activate both families with an E_{max}/EC_{50} value differing by at most 100-fold in (Avet et al., 2022). To investigate how such atypical dual binding may be possible mechanistically, we explored if these receptors share amino acid or property consensus sequences with the above GPCRs with selectivity for either G_s or $G_{i/o}$ ("G protein characteristic" box in Table S5). We find that the promiscuous receptors share 2, 1, and 5 consensus amino acids with the G_s, $G_{i/o}$ and both families, respectively. Furthermore, they share 6, 2, and 8 consensus properties with the G_s, $G_{i/o}$ and both families, respectively. These findings suggest that receptors that activate both G_s and $G_{i/o}$ do so by combining conserved residue properties with a mix of G_s- and $G_{i/o}$-specific properties. Such activation would entail yet uncharacterized receptor interfaces that match both, G_s and $G_{i/o}$ proteins.

DISCUSSION

It is of fundamental importance to understand how members of the same GPCR family bind different G proteins in a selective or promiscuous manner. In this paper, we report four cryo-EM structures of 5-HT_4-G_s, 5-HT_6-G_s, 5-HT_7-G_s, and 5-HT_4-G_i complexes. The structures, together with mutagenesis studies, reveal features of ligand binding pockets that determine serotonin pan-agonism for serotonin receptors and 5-CT preference for 5-HT_7 receptor. Importantly, these structures also reveal a macro-switch formed by alternating TM5-TM6 lengths that determines G_s-over-$G_{i/o}$ selectivity at the receptor level. Comparison of G_s- and $G_{i/o}$-coupled structures revealed that this TM5-TM6 length switch is common for many class A GPCRs. However, this switch may not be conserved in other GPCR classes. TM6 has been described as switch for activation (involving binding of any G protein) but differs in its mechanism spanning helix toggling, rotation and unwinding across the different GPCR classes (Kooistra et al.). In class B1 receptors, TM6 unwinds at its the extracellular-facing half (Hilger et al., 2020; Liang et al., 2020; Zhang et al., 2020) and in class C receptors, this helix only has a small cytosolic movement and rotation (Mao et al., 2020).

Furthermore, the TM5-TM6 length switch acting as a primary G protein selectivity determinant also promotes specific receptor-G protein interactions, defined as "micro-switches," which are present in the cytosolic interface to determine the selective binding of the G_s- or $G_{i/o}$ families of G proteins. In comparison, a mainly sequence-based GPCR-G protein selectivity study suggested a shape-matching mechanism involving complementary "ridges" and "grooves" at the receptor-G protein

interface, but it did not identify conserved receptor residues mediating selective coupling (Flock et al., 2017). Notably, such residue micro-switches were not discernable upon publication of the first $G_{i/o}$-bound class A GPCR structures leading to the speculation that such residue determinants may not exist (Capper and Wacker, 2018).

The structure and sequence analyses presented herein reveal that TM5 and TM6 contains specific conserved residues that constitutes the primary G protein selectivity determinants at the receptor level and in their turn create specific contacts to G_s or $G_{i/o}$ proteins. Notably, 83% of the G_s or G_i-specific contacts are to the α5 helix including interactions to all five most C-terminal residues. Furthermore, all three G_i-specific contacts are formed to the two most C-terminal α5 helix residues. This provides a structural explanation to the recent report in which only the six C-terminal amino acids of G_q were mutated to yield 11 distinct chimera that could represent all 16 human G protein subtypes in terms of their coupling profiles to 148 GPCRs (Inoue et al., 2019b). However, we identified 21 contacts critical for G_s selectivity, which is much more than the three specific contacts that convey $G_{i/o}$ selectivity (Figures S4 and S6). This provides the first structural rationale to why the number of human GPCRs that couple to $G_{i/o}$ (161) is almost double as many of GPCRs that couple to G_s (82) (Flock et al., 2017).

Cryo-EM and crystal structures represent snapshots and therefore do not show the intrinsic flexibility that receptors possess to allow them to signal through multiple G protein subtypes. It would therefore be highly valuable to solve structures of the same receptor in complex with G proteins from different families to elucidate the mechanisms of promiscuity. The determination of 5-HT_4 structures with both G_s and G_i revealed major differences in the lengths of TM5 and TM6 across the complexes. These findings emphasize the value of structures with a preserved integrity in the region spanning from the TM5 end via ICL3 to the TM6 end, which has been replaced with a fusion protein in many crystal structures. Such structures with truncated receptor TM5 would lead to the inability to observe the apparent elongation of TM5 or TM6 upon activation (Flock et al., 2017), which features can only be observed in our full-length receptor-G protein complexes.

The first comparisons of G_s- and $G_{i/o}$-coupled receptors became possible upon publication of the first G_i-coupled receptor structures (Draper-Joyce et al., 2018b; Garcia-Nafria et al., 2018c; Kang et al., 2018a; Koehl et al., 2018b). The initial structural comparisons revealed a high level of structural plasticity in receptors' G protein-binding domains and suggested that G protein selectivity arises mainly from ''pocket complementarity'' (Draper-Joyce et al., 2018b) while also supported by alternative patterns of hydrophilic and hydrophobic residues in the interface (Kang et al., 2018a). However, here we propose that this pocket complementary is primarily guided by structural selectivity ''macro-switches'' (i.e., the differential lengths of TM5 and TM6), which uniquely positions ''micro-switches.'' Importantly, these micro-switches have not been readily discernable previously but were identified herein through comparative sequence analyses of specific amino acids rather than properties. Furthermore, the sequence-based identification of selectivity micro-switches was made possible by the first large-scale systematic G protein-coupling datasets (Avet et al., 2022; Inoue et al., 2019b), and a meta-analysis (Hauser et al., 2022) integrating these with the literature annotation in the Guide to Pharmacology database (Harding et al., 2021). We also found that dual G_s- and $G_{i/o}$-coupling receptors combine conserved and specific properties, while further studies will be needed to reveal its structural basis. Such promiscuous activation of G_s and $G_{i/o}$ is the rarest combination of any G protein family pair, and when it occurs it has the highest average difference in log (E_{max}/EC_{50}) values (Hauser et al., 2022). Taken together, the present study greatly expands our mechanistic understanding of G_s versus $G_{i/o}$ family selectivity by revealing a combination of structural and sequence determinants and across the levels of helix macro-switches and residue micro-switches.

Limitations of the study

The promiscuity of G-protein coupling is manifested in many GPCRs. However, the knowledge of the structural determinants of G protein selectivity is limited by the number and qualities of GPCR structures and the structures of GPCRs in complexes with different G-proteins. The TM5-TM6 switches are only partial factor determining the selectivity between G_s and G_i. Uncovering the complicated coupling relationships between multiple GPCRs and G-proteins still requires substantial effort in structural and functional studies.

STAR★METHODS

Detailed methods are provided in the online version of this paper and include the following:

- KEY RESOURCES TABLE
- RESOURCE AVAILABILITY
  - Lead contact
  - Materials availability
  - Data and code availability
- EXPERIMENTAL MODEL AND SUBJECT DETAILS
  - Cell lines
- METHOD DETAILS
  - Constructs
  - Protein complex expression and purification
  - NanoBiT β-arrestin recruitment assay
  - cAMP accumulation assay
  - GloSensor cAMP assay
  - Detection of surface expression of mutants
  - Cryo-EM grid preparation and data collection
  - Image processing and map construction
  - Model building and refinement
  - Selection of representative structures
  - Structure preparation for ligand binding mode analysis
  - Length and angle analyses
  - Receptor-G protein interaction matrices
  - Secondary structure prediction
  - Sequence-based identification of G_s vs. $G_{i/o}$ binding determinants and selectivity residue micro-switches
- QUANTIFICATION AND STATISTICAL ANALYSIS

SUPPLEMENTAL INFORMATION

Supplemental information can be found online at https://doi.org/10.1016/j.molcel.2022.05.031.

ACKNOWLEDGMENTS

The cryo-EM data were collected at the Center of Cryo-Electron Microscopy, Shanghai Institute of Materia Medica, and at the Center of Cryo-Electron Microscopy, Zhejiang University. Cryo-EM data collection for the 5-HT_4-G_s complex was carried out at Shuimu BioSciences Ltd. The authors thank all staff at Shuimu BioSciences Ltd. for their technical support. This work was partially supported by the National Key R&D Programs of China (2018YFA0507002), the Shanghai Municipal Science and Technology Major Project (2019SHZDZX02), the CAS Strategic Priority Research Program (XDB37030103) to H.E.X.; the National Key Basic Research Program of China (2019YFA0508800), the National Natural Science Foundation of China (81922071), the Zhejiang Province Natural Science Fund for Excellent Young Scholars (LR19H310001), Key R & D Projects of Zhejiang Province (2021C03039) to Y.Z.; the National Natural Science Foundation of China (31770796) and National Science and Technology Major Project (2018ZX09711002-002-002) to Y.J.; the EU Horizon 2020, Innovative Training Network SAFER (765657) to I.A.S.; the Lundbeck Foundation (R163-2013-16327) and Novo Nordisk Foundation (NNF18OC0031226) to D.E.G. and K.H. We thank Albert J. Kooistra and Gáspár Pándy-Szekeres for structure annotation, and Henrik Daver for scripts to calculate G protein insertion angles. Cartoons in graphical abstract, Figure 1A, and Figure 6L were created with BioRender.com.

AUTHOR CONTRIBUTIONS

Conceptualization, H.E.X.; Methodology, Formal Analysis, and Visualization, S.H., P.X., D.-D.S., I.A.S., C.M., and Y.T.; Investigation, S.H., P.X., D.-D.S., I.A.S., C.M., Y.T., H.L., Y.Z., C.Y., and X.Y.; Writing – Original Draft, P.X., S.H., I.A.S., D.E.G. and H.E.X.; Writing – Review & Editing, all authors. Funding Acquisition, Y.J., Y.Z., D.E.G., and H.E.X.; Supervision, D.E.G., K.H., Y.Z. and H.E.X.

DECLARATION OF INTERESTS

The authors declare no competing interests.

Received: June 18, 2021
Revised: April 27, 2022
Accepted: May 26, 2022
Published: June 16, 2022

REFERENCES

Adams, P.D., Afonine, P.V., Bunkóczi, G., Chen, V.B., Davis, I.W., Echols, N., Headd, J.J., Hung, L.W., Kapral, G.J., Grosse-Kunstleve, R.W., et al. (2010). PHENIX: a comprehensive Python-based system for macromolecular structure solution. Acta Crystallogr. D. Biol. Crystallogr. *66*, 213–221. https://doi.org/10.1107/s0907444909052925.

Avet, C., Mancini, A., Breton, B., Gouill, C.L., Hauser, A.S., Normand, C., Kobayashi, H., Gross, F., Hogue, M., Lukasheva, V., et al. (2022). Effector membrane translocation biosensors reveal G protein and βarrestin coupling profiles of 100 therapeutically relevant GPCRs. Preprint at bioRxiv. https://doi.org/10.7554/eLife.74101.

Avet, C., Mancini, A., Breton, B., Le Gouill, C., Hauser, A.S., Normand, C., Kobayashi, H., Gross, F., Hogue, M., Lukasheva, V., et al. (2020). Selectivity landscape of 100 therapeutically relevant GPCR profiled by an effector translocation-based BRET platform. Preprint at bioRxiv. https://doi.org/10.1101/2020.04.20.052027.

Berger, M., Gray, J.A., and Roth, B.L. (2009). The expanded biology of serotonin. Annu. Rev. Med. *60*, 355–366. https://doi.org/10.1146/annurev.med.60.042307.110802.

Capper, M.J., and Wacker, D. (2018). How the ubiquitous GPCR receptor family selectively activates signalling pathways. Nature *558*, 529–530. https://doi.org/10.1038/d41586-018-05503-4.

Chen, V.B., Arendall, W.B., Headd, J.J., Keedy, D.A., Immormino, R.M., Kapral, G.J., Murray, L.W., Richardson, J.S., and Richardson, D.C. (2010). MolProbity: all-atom structure validation for macromolecular crystallography. Acta Crystallogr. D *66*, 12–21. https://doi.org/10.1107/s0907444909042073.

Chun, E., Thompson, A.A., Liu, W., Roth, C.B., Griffith, M.T., Katritch, V., Kunken, J., Xu, F., Cherezov, V., Hanson, M.A., and Stevens, R. (2012). Fusion partner toolchest for the stabilization and crystallization of G protein-coupled receptors. Structure *20*, 967–976. https://doi.org/10.1016/j.str.2012.04.010.

Cuff, J.A., and Barton, G.J. (2000). Application of multiple sequence alignment profiles to improve protein secondary structure prediction. Protein Struct. Funct. Genet. *40*, 502–511. https://doi.org/10.1002/1097-0134(20000815)40:3<502::aid-prot170>3.0.co;2-q.

Dixon, A.S., Schwinn, M.K., Hall, M.P., Zimmerman, K., Otto, P., Lubben, T.H., Butler, B.L., Binkowski, B.F., Machleidt, T., Kirkland, T.A., et al. (2016). NanoLuc complementation reporter optimized for accurate measurement of protein interactions in cells. ACS Chem. Biol. *11*, 400–408. https://doi.org/10.1021/acschembio.5b00753.

Draper-Joyce, C.J., Khoshouei, M., Thal, D.M., Liang, Y.L., Nguyen, A.T.N., Furness, S.G.B., Venugopal, H., Baltos, J.A., Plitzko, J.M., Danev, R., et al. (2018a). Structure of the adenosine-bound human adenosine A1 receptor-Gi complex. Nature *558*, 559–563. https://doi.org/10.1038/s41586-018-0236-6.

Draper-Joyce, C.J., Khoshouei, M., Thal, D.M., Liang, Y.L., Nguyen, A.T.N., Furness, S.G.B., Venugopal, H., Baltos, J.A., Plitzko, J.M., Danev, R., et al. (2018b). Structure of the adenosine-bound human adenosine A1 receptor-Gi complex. Nature *558*, 559–563. https://doi.org/10.1038/s41586-018-0236-6.

Drozdetskiy, A., Cole, C., Procter, J., and Barton, G.J. (2015). JPred4: a protein secondary structure prediction server. Nucleic Acids Res. *43*, W389–W394. https://doi.org/10.1093/nar/gkv332.

Du, Y., Duc, N.M., Rasmussen, S.G.F., Hilger, D., Kubiak, X., Wang, L., Bohon, J., Kim, H.R., Wegrecki, M., Asuru, A., et al. (2019). Assembly of a GPCR-G protein complex. Cell *177*, 1232–1242.e11. https://doi.org/10.1016/j.cell.2019.04.022.

Emsley, P., and Cowtan, K. (2004). Coot: model-building tools for molecular graphics. Acta Crystallogr. D. Biol. Crystallogr. *60*, 2126–2132. https://doi.org/10.1107/s0907444904019158.

Emsley, P., Lohkamp, B., Scott, W.G., and Cowtan, K. (2010). Features and development of coot. Acta Crystallogr. D. Biol. Crystallogr. *66*, 486–501. https://doi.org/10.1107/s0907444910007493.

Flock, T., Hauser, A.S., Lund, N., Gloriam, D.E., Balaji, S., and Babu, M.M. (2017). Selectivity determinants of GPCR-G-protein binding. Nature *545*, 317–322. https://doi.org/10.1038/nature22070.

Flock, T., Ravarani, C.N.J., Sun, D., Venkatakrishnan, A.J., Kayikci, M., Tate, C.G., Veprintsev, D.B., and Babu, M.M. (2015). Universal allosteric mechanism for Gα activation by GPCRs. Nature *524*, 173–179. https://doi.org/10.1038/nature14663.

García-Nafría, J., Lee, Y., Bai, X., Carpenter, B., and Tate, C.G. (2018a). Cryo-EM structure of the adenosine A2A receptor coupled to an engineered heterotrimeric G protein. Elife *7*, e35946. https://doi.org/10.7554/elife.35946.

García-Nafría, J., Nehmé, R., Edwards, P.C., and Tate, C.G. (2018b). Cryo-EM structure of the serotonin 5-HT1B receptor coupled to heterotrimeric Go. Nature *558*, 620–623. https://doi.org/10.1038/s41586-018-0241-9.

Garcia-Nafria, J., Nehme, R., Edwards, P.C., and Tate, C.G. (2018c). Cryo-EM structure of the serotonin 5-HT1B receptor coupled to heterotrimeric Go. Nature *558*, 620–623. https://doi.org/10.1038/s41586-018-0241-9.

Greenwood, J.R., Calkins, D., Sullivan, A.P., and Shelley, J.C. (2010). Towards the comprehensive, rapid, and accurate prediction of the favorable tautomeric states of drug-like molecules in aqueous solution. J. Comput. Aided Mol. Des. *24*, 591–604. https://doi.org/10.1007/s10822-010-9349-1.

Harding, S.D., Armstrong, J.F., Faccenda, E., Southan, C., Alexander, S.P.H., Davenport, A.P., Pawson, A.J., Spedding, M., and Davies, J.A.; NC-IUPHAR (2021). The IUPHAR/BPS guide to PHARMACOLOGY in 2022: curating pharmacology for COVID-19, malaria and antibacterials. Nucleic Acids Res. *50*, D1282–D1294. https://doi.org/10.1093/nar/gkab1010.

Hauser, A.S., Avet, C., Normand, C., Mancini, A., Inoue, A., Bouvier, M., and Gloriam, D.E. (2022). Common coupling map advances GPCR-G protein selectivity. Preprint at bioRxiv. https://doi.org/10.1101/2021.09.07.459250.

Hauser, S.R., Hedlund, P.B., Roberts, A.J., Sari, Y., Bell, R.L., and Engleman, E.A. (2015). The 5-HT7 receptor as a potential target for treating drug and alcohol abuse. Front Neurosci-Switz. *8*, 448. https://doi.org/10.3389/fnins.2014.00448.

Heymann, J.B. (2018). Guidelines for using Bsoft for high resolution reconstruction and validation of biomolecular structures from electron micrographs *27*, 159–171. https://doi.org/10.1002/pro.3293.

Hilger, D., Kumar, K.K., Hu, H., Pedersen, M.F., O'Brien, E.S., Giehm, L., Jennings, C., Eskici, G., Inoue, A., Lerch, M., et al. (2020). Structural insights into differences in G protein activation by family A and family B GPCRs. Science *369*, eaba3373. https://doi.org/10.1126/science.aba3373.

Hong, C., Byrne, N.J., Zamlynny, B., Tummala, S., Xiao, L., Shipman, J.M., Partridge, A.T., Minnick, C., Breslin, M.J., Rudd, M.T., et al. (2021). Structures of active-state orexin receptor 2 rationalize peptide and small-molecule agonist recognition and receptor activation. Nat. Commun. *12*, 815. https://doi.org/10.1038/s41467-021-21087-6.

Hua, T., Li, X., Wu, L., Iliopoulos-Tsoutsouvas, C., Wang, Y., Wu, M., Shen, L., Brust, C.A., Nikas, S.P., Song, F., et al. (2020). Activation and signaling mechanism revealed by cannabinoid receptor-Gi complex structures. Cell *180*, 655–665.e18. https://doi.org/10.1016/j.cell.2020.01.008.

Inoue, A., Raimondi, F., Kadji, F.M.N., Singh, G., Kishi, T., Uwamizu, A., Ono, Y., Shinjo, Y., Ishida, S., Arang, N., et al. (2019a). Illuminating G-protein-coupling selectivity of GPCRs. Cell *177*, 1933–1947.e25. https://doi.org/10.1016/j.cell.2019.04.044.

Inoue, A., Raimondi, F., Kadji, F.M.N., Singh, G., Kishi, T., Uwamizu, A., Ono, Y., Shinjo, Y., Ishida, S., Arang, N., et al. (2019b). Illuminating G-protein-coupling selectivity of GPCRs. Cell *177*, 1933–1947.e25. e1925. https://doi.org/10.1016/j.cell.2019.04.044.

Isberg, V., de Graaf, C., Bortolato, A., Cherezov, V., Katritch, V., Marshall, F.H., Mordalski, S., Pin, J.P., Stevens, R.C., Vriend, G., and Gloriam, D.E. (2015). Generic GPCR residue numbers - aligning topology maps while minding the gaps. Trends Pharmacol. Sci. *36*, 22–31. https://doi.org/10.1016/j.tips.2014.11.001.

Isberg, V., Mordalski, S., Munk, C., Rataj, K., Harpsøe, K., Hauser, A.S., Vroling, B., Bojarski, A.J., Vriend, G., and Gloriam, D.E. (2016). GPCRdb: an information system for G protein-coupled receptors. Nucleic Acids Res. *45*, 2936. https://doi.org/10.1093/nar/gkw1218.

Isberg, V., Vroling, B., van der Kant, R., Li, K., Vriend, G., and Gloriam, D. (2014). GPCRDB: an information system for G protein-coupled receptors. Nucleic Acids Res. *42*, D422–D425. https://doi.org/10.1093/nar/gkt1255.

Israeli, H., Degtjarik, O., Fierro, F., Chunilal, V., Gill, A.K., Roth, N.J., Botta, J., Prabahar, V., Peleg, Y., Chan, L.F., et al. (2021). Structure reveals the activation mechanism of the MC4 receptor to initiate satiation signaling. Science *372*, 808–814. https://doi.org/10.1126/science.abf7958.

Kang, Y., Kuybeda, O., de Waal, P.W., Mukherjee, S., Van Eps, N., Dutka, P., Zhou, X.E., Bartesaghi, A., Erramilli, S., Morizumi, T., et al. (2018a). Cryo-EM structure of human rhodopsin bound to an inhibitory G protein. Nature *558*, 553–558. https://doi.org/10.1038/s41586-018-0215-y.

Kang, Y.Y., Kuybeda, O., de Waal, P.W., Mukherjee, S., Van Eps, N., Dutka, P., Zhou, X.E., Bartesaghi, A., Erramilli, S., Morizumi, T., et al. (2018b). Cryo-EM structure of human rhodopsin bound to an inhibitory G protein. Nature *558*, 553. https://doi.org/10.1038/s41586-018-0215-y.

Kato, H.E., Zhang, Y., Hu, H., Suomivuori, C.M., Kadji, F.M.N., Aoki, J., Krishna Kumar, K., Fonseca, R., Hilger, D., Huang, W., et al. (2019). Conformational transitions of a neurotensin receptor 1-Gi1 complex. Nature *572*, 80–85. https://doi.org/10.1038/s41586-019-1337-6.

Kim, K., Che, T., Panova, O., DiBerto, J.F., Lyu, J., Krumm, B.E., Wacker, D., Robertson, M.J., Seven, A.B., Nichols, D.E., et al. (2020). Structure of a hallucinogen-activated Gq-coupled 5-HT2A serotonin receptor. Cell *182*, 1574–1588.e19. https://doi.org/10.1016/j.cell.2020.08.024.

Koehl, A., Hu, H., Maeda, S., Zhang, Y., Qu, Q., Paggi, J.M., Latorraca, N.R., Hilger, D., Dawson, R., Matile, H., et al. (2018a). Structure of the μ-opioid receptor–Gi protein complex. Nature *558*, 547–552. https://doi.org/10.1038/s41586-018-0219-7.

Koehl, A., Hu, H., Maeda, S., Zhang, Y., Qu, Q., Paggi, J.M., Latorraca, N.R., Hilger, D., Dawson, R., Matile, H., et al. (2018b). Structure of the micro-opioid receptor-Gi protein complex. Nature *558*, 547–552. https://doi.org/10.1038/s41586-018-0219-7.

Kooistra, A.J., Mordalski, S., Pándy-Szekeres, G., Esguerra, M., Mamyrbekov, A., Munk, C., Keserű, G.M., and Gloriam, D.E. (2021). GPCRdb in 2021: integrating GPCR sequence, structure and function. Nucleic Acids Res. *49*, D335–D343. https://doi.org/10.1093/nar/gkaa1080.

Kooistra, A.J., Munk, C., Hauser, A.S., Babu, M.M., and Gloriam, D.E. GPCR activation mechanisms across classes and macro/microscales. In review.

Liang, Y.L., Belousoff, M.J., Zhao, P., Koole, C., Fletcher, M.M., Truong, T.T., Julita, V., Christopoulos, G., Xu, H.E., Zhang, Y., et al. (2020). Toward a structural understanding of class B GPCR peptide binding and activation. Mol. Cell *77*, 656–668.e5. https://doi.org/10.1016/j.molcel.2020.01.012.

Liang, Y.L., Zhao, P., Draper-Joyce, C., Baltos, J.A., Glukhova, A., Truong, T.T., May, L.T., Christopoulos, A., Wootten, D., Sexton, P.M., and Furness, S.G.B. (2018). Dominant negative G proteins enhance formation and purification of agonist-GPCR-G protein complexes for structure determination. ACS Pharmacol. Transl. Sci. *1*, 12–20. https://doi.org/10.1021/acsptsci.8b00017.

Lin, X., Li, M., Wang, N., Wu, Y., Luo, Z., Guo, S., Han, G.W., Li, S., Yue, Y., Wei, X., et al. (2020). Structural basis of ligand recognition and self-activation of orphan GPR52. Nature *579*, 152–157. https://doi.org/10.1038/s41586-020-2019-0.

Liu, K., Wu, L., Yuan, S., Wu, M., Xu, Y., Sun, Q., Li, S., Zhao, S., Hua, T., and Liu, Z.J. (2020). Structural basis of CXC chemokine receptor 2 activation and signalling. Nature *585*, 135–140. https://doi.org/10.1038/s41586-020-2492-5.

Liu, P., Jia, M.-z., Zhou, X.E., De Waal, P.W., Dickson, B.M., Liu, B., Hou, L., Yin, Y.-t., Kang, Y.-y., Shi, Y., et al. (2016). The structural basis of the dominant negative phenotype of the Gαi1β1γ2 G203A/A326S heterotrimer. Acta Pharmacol. Sin. *37*, 1259–1272. https://doi.org/10.1038/aps.2016.69.

Liu, P., Yin, Y.L., Wang, T., Hou, L., Wang, X.X., Wang, M., Zhao, G.G., Shi, Y., Xu, H.E., and Jiang, Y. (2019a). Ligand-induced activation of ERK1/2 signaling by constitutively active Gs-coupled 5-HT receptors. Acta Pharmacol. Sin. *40*, 1157–1167. https://doi.org/10.1038/s41401-018-0204-6.

Liu, P., Yin, Y.L., Wang, T., Hou, L., Wang, X.X., Wang, M., Zhao, G.G., Shi, Y., Xu, H.E., and Jiang, Y. (2019b). Ligand-induced activation of ERK1/2 signaling by constitutively active Gs-coupled 5-HT receptors. Acta Pharmacol. Sin. *40*, 1157–1167. https://doi.org/10.1038/s41401-018-0204-6.

Maeda, S., Koehl, A., Matile, H., Hu, H., Hilger, D., Schertler, G.F.X., Manglik, A., Skiniotis, G., Dawson, R.J.P., and Kobilka, B.K. (2018). Development of an antibody fragment that stabilizes GPCR/G-protein complexes. Nat. Commun. *9*, 3712. https://doi.org/10.1038/s41467-018-06002-w.

Maeda, S., Qu, Q., Robertson, M.J., Skiniotis, G., and Kobilka, B.K. (2019). Structures of the M1 and M2 muscarinic acetylcholine receptor/G-protein complexes. Science *364*, 552–557. https://doi.org/10.1126/science.aaw5188.

Manabe, N., Wong, B.S., and Camilleri, M. (2010). New-generation 5-HT4 receptor agonists: potential for treatment of gastrointestinal motility disorders. Expert Opin. Inv. Drug *19*, 765–775. https://doi.org/10.1517/13543784.2010.482927.

Mao, C., Shen, C., Li, C., Shen, D.D., Xu, C., Zhang, S., Zhou, R., Shen, Q., Chen, L.N., Jiang, Z., et al. (2020). Cryo-EM structures of inactive and active GABAB receptor. Cell Res. *30*, 564–573. https://doi.org/10.1038/s41422-020-0350-5.

Mastronarde, D.N. (2005). Automated electron microscope tomography using robust prediction of specimen movements *152*, 36–51. https://doi.org/10.1016/j.jsb.2005.07.007.

Mitchell, E.S., and Neumaier, J.F. (2005). 5-HT6 receptors: a novel target for cognitive enhancement. Pharmacol. Ther. *108*, 320–333. https://doi.org/10.1016/j.pharmthera.2005.05.001.

Munk, C., Isberg, V., Mordalski, S., Harpsøe, K., Rataj, K., Hauser, A.S., Kolb, P., Bojarski, A.J., Vriend, G., and Gloriam, D.E. (2016). GPCRdb: the G protein-coupled receptor database - an introduction. Br. J. Pharmacol. *173*, 2195–2207. https://doi.org/10.1111/bph.13509.

Nandam, L.S., Jhaveri, D., and Bartlett, P. (2007). 5-HT7, neurogenesis and antidepressants: a promising therapeutic axis for treating depression. Clin. Exp. Pharmacol. Physiol. *34*, 546–551. https://doi.org/10.1111/j.1440-1681.2007.04608.x.

Nichols, D.E., and Nichols, C.D. (2008). Serotonin receptors. Chem. Rev. *108*, 1614–1641. https://doi.org/10.1021/cr078224o.

Nojima, S., Fujita, Y., Kimura, K.T., Nomura, N., Suno, R., Morimoto, K., Yamamoto, M., Noda, T., Iwata, S., Shigematsu, H., and Kobayashi, T. (2021). Cryo-EM structure of the prostaglandin E receptor EP4 coupled to G protein. Structure *29*, 252–260.e6. https://doi.org/10.1016/j.str.2020.11.007.

Olsson, M.H.M., Søndergaard, C.R., Rostkowski, M., and Jensen, J.H. (2011). PROPKA3: consistent treatment of internal and surface residues in empirical pKa predictions. J. Chem. Theory. Comput. *7*, 525–537. https://doi.org/10.1021/ct100578z.

Pauwels, P.J. (2000). Diverse signalling by 5-hydroxytryptamine (5-HT) receptors. Biochem. Pharmacol. *60*, 1743–1750. https://doi.org/10.1016/s0006-2952(00)00476-7.

Pettersen, E.F., Goddard, T.D., Huang, C.C., Couch, G.S., Greenblatt, D.M., Meng, E.C., and Ferrin, T.E. (2004). UCSF Chimera–a visualization system for exploratory research and analysis. J. Comput. Chem. *25*, 1605–1612. https://doi.org/10.1002/jcc.20084.

Pettersen, E.F., Goddard, T.D., Huang, C.C., Meng, E.C., Couch, G.S., Croll, T.I., Morris, J.H., and Ferrin, T.E. (2020). UCSF ChimeraX: structure visualization for researchers, educators, and developers. Protein Sci. *30*, 70–82. https://doi.org/10.1002/pro.3943.

Pindon, A., Van Hecke, G., Van Gompel, P., Lesage, A.S., Leysen, J.E., and Jurzak, M. (2002). Differences in signal transduction of two 5-HT4Receptor splice variants: compound specificity and dual coupling with Gαs-and Gαi/o-proteins. Mol. Pharmacol. *61*, 85–96. https://doi.org/10.1124/mol.61.1.85.

Rasmussen, S.G.F., DeVree, B.T., Zou, Y., Kruse, A.C., Chung, K.Y., Kobilka, T.S., Thian, F.S., Chae, P.S., Pardon, E., Calinski, D., et al. (2011a). Crystal structure of the β2 adrenergic receptor–Gs protein complex. Nature *477*, 549–555. https://doi.org/10.1038/nature10361.

Rasmussen, S.G.F., DeVree, B.T., Zou, Y., Kruse, A.C., Chung, K.Y., Kobilka, T.S., Thian, F.S., Chae, P.S., Pardon, E., Calinski, D., et al. (2011b). Crystal structure of the beta2 adrenergic receptor-Gs protein complex. Nature *477*, 549–555. https://doi.org/10.1038/nature10361.

Roos, K., Wu, C., Damm, W., Reboul, M., Stevenson, J.M., Lu, C., Dahlgren, M.K., Mondal, S., Chen, W., Wang, L., et al. (2019). OPLS3e: extending Force Field Coverage for Drug-Like Small Molecules. J. Chem. Theory Comput. *15*, 1863–1874. https://doi.org/10.1021/acs.jctc.8b01026.

Sanchez-Garcia, R., Gomez-Blanco, J., Cuervo, A., Carazo, J.M., Sorzano, C.O.S., and Vargas, J. (2021). DeepEMhancer: a deep learning solution for cryo-EM volume post-processing. Commun. Biol. *4*, 874. https://doi.org/10.1038/s42003-021-02399-1.

Sastry, G.M., Adzhigirey, M., Day, T., Annabhimoju, R., and Sherman, W. (2013). Protein and ligand preparation: parameters, protocols, and influence on virtual screening enrichments. J. Comput. Aided Mol. Des. *27*, 221–234. https://doi.org/10.1007/s10822-013-9644-8.

Scheres, S.H.W. (2012). RELION: implementation of a Bayesian approach to cryo-EM structure determination. J. Struct. Biol. *180*, 519–530. https://doi.org/10.1016/j.jsb.2012.09.006.

Sharp, T., and Barnes, N.M. (2020). Central 5-HT receptors and their function; present and future. Neuropharmacology *177*, 108155. https://doi.org/10.1016/j.neuropharm.2020.108155.

Shelley, J.C., Cholleti, A., Frye, L.L., Greenwood, J.R., Timlin, M.R., and Uchimaya, M. (2007). Epik: a software program for pK(a) prediction and protonation state generation for drug-like molecules. J. Comput. Aided Mol. Des. *21*, 681–691. https://doi.org/10.1007/s10822-007-9133-z.

Søndergaard, C.R., Olsson, M.H.M., Rostkowski, M., and Jensen, J.H. (2011). Improved treatment of ligands and coupling effects in empirical calculation and rationalization of pKa values. J. Chem. Theory Comput. *7*, 2284–2295. https://doi.org/10.1021/ct200133y.

Su, M., Zhu, L., Zhang, Y., Paknejad, N., Dey, R., Huang, J., Lee, M.Y., Williams, D., Jordan, K.D., Eng, E.T., et al. (2020). Structural basis of the activation of heterotrimeric Gs-protein by Isoproterenol-bound β1-adrenergic receptor. Mol. Cell *80*, 59–71.e4. https://doi.org/10.1016/j.molcel.2020.08.001.

Vass, M., Podlewska, S., de Esch, I.J.P., Bojarski, A.J., Leurs, R., Kooistra, A.J., and de Graaf, C. (2019). Aminergic GPCR-ligand interactions: a chemical and structural map of receptor mutation data. J. Med. Chem. *62*, 3784–3839. https://doi.org/10.1021/acs.jmedchem.8b00836.

Wasilko, D.J., Johnson, Z.L., Ammirati, M., Che, Y., Griffor, M.C., Han, S., and Wu, H. (2020). Structural basis for chemokine receptor CCR6 activation by the endogenous protein ligand CCL20. Nat. Commun. *11*, 3031. https://doi.org/10.1038/s41467-020-16820-6.

Xia, R., Wang, N., Xu, Z., Lu, Y., Song, J., Zhang, A., Guo, C., and He, Y. (2021). Cryo-EM structure of the human histamine H1 receptor/Gq complex. Nat. Commun. *12*, 2086. https://doi.org/10.1038/s41467-021-22427-2.

Xing, C., Zhuang, Y., Xu, T.H., Feng, Z., Zhou, X.E., Chen, M., Wang, L., Meng, X., Xue, Y., Wang, J., et al. (2020). Cryo-EM structure of the human cannabinoid receptor CB2-Gi signaling complex. Cell *180*, 645–654.e13. https://doi.org/10.1016/j.cell.2020.01.007.

Xu, P., Huang, S., Mao, C., Krumm, B.E., Zhou, X.E., Tan, Y., Huang, X.P., Liu, Y., Shen, D.D., Jiang, Y., et al. (2021a). Structures of the human dopamine D3 receptor-Gi complexes. Mol. Cell *81*, 1147–1159.e4. https://doi.org/10.1016/j.molcel.2021.01.003.

Xu, P., Huang, S., Zhang, H., Mao, C., Zhou, X.E., Cheng, X., Simon, I.A., Shen, D.D., Yen, H.Y., Robinson, C.V., et al. (2021b). Structural insights into the lipid and ligand regulation of serotonin receptors. Nature *592*, 469–473. https://doi.org/10.1038/s41586-021-03376-8.

Yamada, J., Sugimoto, Y., Noma, T., and Yoshikawa, T. (1998). Effects of the non-selective 5-HT receptor agonist, 5-carboxamidotryptamine, on plasma glucose levels in rats. Eur. J. Pharmacol. *359*, 81–86. https://doi.org/10.1016/s0014-2999(98)00617-7.

Yang, F., Mao, C., Guo, L., Lin, J., Ming, Q., Xiao, P., Wu, X., Shen, Q., Guo, S., Shen, D.D., et al. (2020). Structural basis of GPBAR activation and bile acid recognition. Nature *587*, 499–504. https://doi.org/10.1038/s41586-020-2569-1.

Yi-Lynn, L., Zhao, P., Draper-Joyce, C., Baltos, J.A., Glukhova, A., Truong, T.T., May, L.T., Christopoulos, A., Wootten, D., Sexton, P.M., and Furness, S.G.B. (2018). Dominant negative G proteins enhance formation and purification of agonist-GPCR-G protein complexes for structure determination. ACS Pharmacol. Transl. Sci. *1*, 12–20. https://doi.org/10.1021/acsptsci.8b00017.

Yuan, D., Liu, Z., Kaindl, J., Maeda, S., Zhao, J., Sun, X., Xu, J., Gmeiner, P., Wang, H.W., and Kobilka, B.K. (2020). Activation of the α2B adrenoceptor by the sedative sympatholytic dexmedetomidine. Nat. Chem. Biol. *16*, 507–512. https://doi.org/10.1038/s41589-020-0492-2.

Zhang, K. (2016). Gctf: Real-time CTF determination and correction. J. Struct. Biol. *193*, 1–12. https://doi.org/10.1016/j.jsb.2015.11.003.

Zhang, X., Belousoff, M.J., Zhao, P., Kooistra, A.J., Truong, T.T., Ang, S.Y., Underwood, C.R., Egebjerg, T., Senel, P., Stewart, G.D., et al. (2020). Differential GLP-1R binding and activation by peptide and non-peptide agonists. Mol. Cell *80*, 485–500.e7. https://doi.org/10.1016/j.molcel.2020.09.020.

Zheng, S.Q., Palovcak, E., Armache, J.P., Verba, K.A., Cheng, Y.F., and Agard, D.A. (2017). MotionCor2: anisotropic correction of beam-induced motion for

improved cryo-electron microscopy. Nat. Methods *14*, 331–332. https://doi.org/10.1038/nmeth.4193.

Zhuang, Y., Liu, H., Edward Zhou, X., Kumar Verma, R., de Waal, P.W., Jang, W., Xu, T.H., Wang, L., Meng, X., Zhao, G., et al. (2020). Structure of formyl-peptide receptor 2-Gi complex reveals insights into ligand recognition and signaling. Nat. Commun. *11*, 885. https://doi.org/10.1038/s41467-020-14728-9.

Zhuang, Y., Xu, P., Mao, C., Wang, L., Krumm, B., Zhou, X.E., Huang, S., Liu, H., Cheng, X., Huang, X.P., et al. (2021). Structural insights into the human D1 and D2 dopamine receptor signaling complexes. Cell *184*, 931–942.e18. https://doi.org/10.1016/j.cell.2021.01.027.

Zivanov, J., Nakane, T., Forsberg, B.O., Kimanius, D., Hagen, W.J.H., Lindahl, E., and Scheres, S.H.W. (2018). New tools for automated high-resolution cryo-EM structure determination in RELION-3. Elife *7*, e42166. https://doi.org/10.7554/elife.42166.

STAR★METHODS

KEY RESOURCES TABLE

REAGENT or RESOURCE	SOURCE	IDENTIFIER
Antibodies		
Anti-Flag Antibody	Sigma Aldrich	Cat# A8592; RRID: AB_439702
Anti-mouse Alexa-488-conjugated secondary antibody	Thermo Fisher Scientific	Cat# A32766; RRID: AB_2762823
gp64-PE antibody	Expression systems	Cat# 97-201
Bacterial and Virus Strains		
*E.*coli strain BL21 (DE3)	NEB	Cat# C2527
Chemicals, Peptides, and Recombinant Proteins		
Protease Inhibitor Cocktail, EDTA-free	Bimake	Cat# B14003
Apyrase	Sigma-Aldrich	Cat# A3162
n-Dodecyl b-D-maltoside (DDM)	Anatrace	Cat# D310
Lauryl maltose neopentyglycol (LMNG)	Anatrace	Cat# NG310
Cholesterol hemisucinate (CHS)	Anatrace	Cat# CH210
Glyco-diosgenin (GDN)	Anatrace	Cat# GDN101
Talon resin	Takara	Cat# 635504
Forskolin	Sigma	Cat# F6886
ESF921 culture medium	Expression systems	Cat# 96-001-01
DMEM/high Glucose medium	GE Healthcare	Cat# SH30243.01
Fetal bovine serum (FBS)	Gemini	Cat# 900-108
Dialyzed FBS	Omega Scientific	Cat# FB-03
Cell adherent reagent	Applygen	Cat# C1010
Serotonin	TargetMol	Cat# 153-98-0
5-CT	Tocris	Cat# 0458
FuGENE® HD transfection reagent	Promega	Cat# E2312
HBSS	Invitrogen	Cat# 14065-056
Imidazole	Sigma	Cat# I0250
BSA	Sigma	Cat# 9048-46-8
Critical Commercial Assays		
Bac to Bac system	Invitrogen	Cat# A11098
NanoBiT PPI Starter Systems	Promega	Cat# N2014
LANCE cAMP kit	PerkinElmer	Cat# TRF0263
GloSensor^{TM} cAMP Assay	Promega	Cat# PRE1291
Deposited Data		
5-HT-5-HT$_4$-G$_S$-Nb35 coordinates	This paper	PDB: 7XT8
5-HT-5-HT$_4$-G$_S$-Nb35 EM map	This paper	EMD-33442
5-HT-5-HT$_4$-G$_S$ coordinates	This paper	PDB: 7XT9
5-HT-5-HT$_4$-G$_S$ EM map	This paper	EMD-33443
5-HT-5-HT$_4$-G$_i$-scFv16 coordinates	This paper	PDB: 7XTA
5-HT-5-HT$_4$-G$_i$-scFv16 EM map	This paper	EMD-33444
5-HT-5-HT$_6$-G$_S$-Nb35 coordinates	This paper	PDB: 7XTB
5-HT-5-HT$_6$-G$_S$-Nb35 EM map	This paper	EMD-33445
5-CT-5-HT$_7$-G$_S$-Nb35 coordinates	This paper	PDB: 7XTC
5-CT-5-HT$_7$R-G$_S$-Nb35 EM map	This paper	EMD-33446
Experimental Models: Cell Lines		

(*Continued on next page*)

Continued

REAGENT or RESOURCE	SOURCE	IDENTIFIER
Insect cell line Sf9	Expression systems	N/A
HEK293T cell line	ATCC	CRL-11268
Insect cell line Hi5	Expression systems	N/A
Recombinant DNA		
pFastBac-HA-FLAG-BRIL-5-HT_4	This paper	N/A
pcDNA6-HA-FLAG-5-HT_4	This paper	N/A
pBiT1.1-HA-5-HT_4-LgBiT	This paper	N/A
pFastBac-HA-FLAG-BRIL-5-HT_6	This paper	N/A
pcDNA6-HA-FLAG-5-HT_6	This paper	N/A
pBiT1.1-HA-5-HT_6-LgBiT	This paper	N/A
pFastBac-HA-FLAG-BRIL-5-HT_7	This paper	N/A
pcDNA6-HA-FLAG-5-HT_7	This paper	N/A
pcDNA6-HA-FLAG-5-HT_{1A}	This paper	N/A
pBiT2.1-SmBiT-β-arrestin2	This paper	N/A
pFastBac-DNGα_i	This paper	N/A
pFastBac-DNGα_s	This paper	N/A
pFastBac-Gβ_1	This paper	N/A
pFastBac-Gγ_2	This paper	N/A
pMESy4-Nb35	(Rasmussen et al., 2011a)	N/A
pFastBac-scFv16-(H8)	This paper	N/A
Software and Algorithms		
MotionCor2	(Zheng et al., 2017)	https://emcore.ucsf.edu/ucsf-software
GCTF	(Zhang, 2016)	https://www2.mrc-lmb.cam.ac.uk/ research/locally-developed-software/ zhang-software/
RELION-3.0	(Zivanov et al., 2018)	https://www3.mrc-lmb.cam.ac.uk/relion/index.php/Download_&_install
Chimera	(Pettersen et al., 2004)	http://www.rbvi.ucsf.edu/chimera/
ChimeraX	(Pettersen et al., 2020)	https://www.cgl.ucsf.edu/chimerax/
COOT	(Emsley et al., 2010)	https://www2.mrc-lmb.cam.ac.uk/personal/pemsley/coot/
Phenix	(Adams et al., 2010)	https://www.phenix-online.org/
GraphPad Prism	GraphPad	https://www.graphpad.com/scientific-software/prism/
Adobe Illustrator CC	Adobe	https://www.adobe.com/

RESOURCE AVAILABILITY

Lead contact

Further information and requests for resources and reagents should be directed to and will be fulfilled by the lead contact, H. Eric Xu (eric.xu@simm.ac.cn).

Materials availability

All unique/stable reagents generated in this study are available from the lead contact without restriction. Plasmids and strains are available from the authors upon request.

Data and code availability

- The atomic coordinates and cryo-EM maps included in this study have been deposited in the Protein Data Bank and Electron Microscopy Data Bank, respectively. PDB: 7XT8 and EMDB: EMD-33442 (5-HT_4-G_s-Nb35-5-HT), PDB: 7XT9 and EMDB: EMD-33443 (5-HT_4-G_s-5-HT); PDB: 7XTA and EMDB: EMD-33444 (5-HT_4-G_i-5-HT); PDB: 7XTB and EMDB: EMD-33445 (5-HT_6-G_s-Nb35-5-HT); PDB: 7XTC and EMDB: EMD-33446 (5-HT_7-G_S-Nb35-5-CT).
- This paper does not report original code.

- Any additional information required to reanalyze the data reported in this paper is available from the lead contact upon request.

EXPERIMENTAL MODEL AND SUBJECT DETAILS

Cell lines

Spodoptera frugiperda (Sf9, Expression systems) and *Trichoplusia ni.* (High Five, Thermo Fisher) cells were grown in ESF 921 medium at 27°C and 120 rpm. HEKT cells were grown in a humidified 37°C incubator with 5% CO_2 using media supplemented with 100 I.U./mL penicillin and100 mg/mL streptomycin (Invitrogen). The human cell lines HEK293T were maintained in DMEM (VWR) con-taining 10% fetal bovine serum (FBS, VWR).

METHOD DETAILS

Constructs

The full-length gene sequences of wild type *human* 5-HT_4, 5-HT_6, and 5-HT_7 receptors were subcloned into pFastbac vector using ClonExpress II One Step Cloning Kit (Vazyme Biotech Co.,Ltd). An N-terminal thermally stabilized BRIL (Chun et al., 2012) as fusion protein to enhance receptor expression, along with N-terminal Flag tag and 8×His tag to facilitate protein purification. For structures determination of 5-HT_4-, 5-HT_6-, and 5-HT_7-G_s complex, a dominant-negative (DN) $G\alpha_s$ format including mutations S54N, G226A, E268A, N271K, K274D, R280K, T284D, and I285T was constructed to decrease the affinity of nucleotide-binding and increase the stability of $G\alpha\beta\gamma$ complex (Yi-Lynn et al., 2018). All the three G_s subunits, human DN_$G\alpha_s$, wild type $G\beta_1$, and $G\gamma_2$ were cloned into the pFastBac vector separately.

Protein complex expression and purification

Human 5-HT_4, 5-HT_6, and 5-HT_7 were separately co-expressed with the three G_s subunits in Sf9 insect cells using the Bac-to-Bac Baculovirus Expression System (Invitrogen). In addition, The 5-HT_4, DN_$G\alpha_i$, $G\beta_1$, $G\gamma_2$, and scFv16 were co-expressed in High Five insect cells. Cell cultures were grown in ESF 921 medium (Expression Systems) to a density of 2.5×10^6 cell/mL and then infected with the corresponding viruses. Cell culture was collected by centrifugation 48 h post-infection and stored at −80°C until use.

For the purification of complex, Cell pellets were thawed in 20 mM HEPES pH 7.4, 50 mM NaCl, 10 mM $MgCl_2$ supplemented with Protease Inhibitor Cocktail (Bimake). The 5-HT_4 and 5-HT_6 complex formation were initiated by addition of 10 μM serotonin (TargetMol), 10 μg/mL Nb35(Rasmussen et al., 2011b), as well as apyrase (25 mU/ml, Sigma); The 5-HT_7 complex formation was initiated by addition of 10 μM 5-CT (Tocris), 10 μg/mL Nb35, as well as apyrase (25 mU/ml, Sigma). The suspension were incubated for 1 h at room temperature and the complex was solubilized from the membrane using 0.5% (w/v) n-dodecyl-β-d-maltoside (DDM, Anatrace) and 0.1% (w/v) cholesteryl hemisuccinate (CHS, Anatrace) for 2 h at 4°C. Insoluble material was removed by centrifugation at 65,000 g for 30 min and the solubilized complex was immobilized by batch binding to Talon affinity resin. After that, the resin was packed and washed with 20 column volumes of 20 mM HEPES pH 7.4, 100 mM NaCl, 5 mM $MgCl_2$, 25 mM imidazole, 10 μM ligands, 0.01% (w/v) LMNG, and 0.002% (w/v) CHS. Finally, the complex was eluted in buffer containing 300 mM imidazole and concentrated using an Amicon Ultra Centrifugal Filter (MWCO 100 kDa). Complex were subjected to size-exclusion chromatography on a Superdex 200 Increase 10/300 column (GE Healthcare) pre-equilibrated with 20 mM HEPES pH 7.4, 100 mM NaCl, 20 μM ligands, 0.00075% (w/v) LMNG, and 0.00025% (w/v) CHS to separate complex from contaminants. Eluted fractions consisting of receptor and G_s-protein complex were pooled and concentrated.

NanoBiT β-arrestin recruitment assay

As the 5-HT_4 and 5-HT_6 exhibit high basal activity in the G_s pathway and hard to detect the concentration-response of 5-HT by the G_s dependent cAMP assay, we used β-arrestin recruitment assay for mutagenesis data. The recruitment of 5-HT_4 and 5-HT6 to β-arrestin were detected in AD293 cells using a NanoBiT assay kit from Promega. NanoBiT is a two-subunit protein complementation system based on NanoLuc luciferase that can be used for intracellular detection of binding and dissociation of GPCRs and G proteins (Dixon et al., 2016). The 17.6 kDa LgBiT fragment of NanoBiT luciferase was fused to the GPCR C-termini via a 15-amino acid flexible linker. SmBiT was N-terminally fused to the β-arrestin2 with a 15-amino acid flexible linker.

The full-length 5-HT_4-LgBiT, 5-HT_6-LgBiT were cloned into pBiT1.1 vector (Invitrogen) with a FLAG tag at its N-terminal, and SmBiT-β-arrestin2 was cloned into pBiT2.1 vector (Invitrogen). AD293 cells were cultured in DMEM High Glucose Medium containing 10% (v/v) fetal bovine serum (FBS) (Life Technologies) at 37°C in a 5% CO_2 incubator. A day before transfection, AD293 cells were plated in a 6-well plate at a density of 5×10^5 cells per well in DMEM supplemented with 1% dialyzed FBS. Cells were grown overnight, and then transfected with 1.5 μg 5-HTR and 1.5 μg β-arrestin2 construct by FuGENE® HD transfection reagent (FuGENE® HD/DNA ratio of 3:1) in each well. After 24 h, the transfected cells were seeded onto 384-well microtiter plates (8,000 cells per well). The NanoBiT PPI luminescence measurement was measured using the Nano-Glo Live Cell Assay System (Promega) according to the manufacturer's instructions. The luminescence measurement upon drug stimulation was taken after measuring the baseline luminescence. Results were analyzed using GraphPad Prism 8.0 (Graphpad Software Inc., San Diego, CA) using "log(agonist) vs. response (three parameters)". Data presented are means ± SEM of at least three independent experiments.

cAMP accumulation assay

The full-length 5-HT_6, and 5-HT_7 were cloned into pcDNA6.0 vector (Invitrogen) with a FLAG tag at its N-terminal. AD293 cells were cultured in DMEM supplemented with 10% (v/v) FBS at 37°C in a 5% CO_2 incubator. The day before transfection, AD293 cells were plated at a density of 2 × 10^5 cells per well in a 12-well plate in DMEM containing 1% dialyzed FBS. Cells were grown overnight and then transfected with 1 μg 5-HTR constructs by FuGENE® HD transfection reagent (FuGENE® HD/DNA ratio of 3:1) in each well. After 24 h, the transfected cells were seeded onto 384-well microtiter plates (3,000 cells/well). cAMP accumulation was performed using the LANCE cAMP kit (PerkinElmer) according to the manufacturer's instructions with different concentrations of peptides. Fluorescence signals were then measured at 620 nm and 665 nm by an Envision multilabel plate reader (PerkinElmer). Data presented are means ± SEM of at least three independent experiments.

GloSensor cAMP assay

The full-length and engineered 5-HT_4, 5-HT_6, 5-HT_7, and 5-HT_{1A} were cloned into pcDNA6.0 vector (Invitrogen) with a FLAG tag at its N-terminal. The day before transfection, AD293 cells were plated in a 6-well plate in DMEM containing 1% dialyzed FBS. Cells were grown overnight and then transfected with a plasmid mixture consisting of 5-HTR constructs and the cAMP biosensor GloSensor-22F (Promega) at a ratio of 3:1. After 24 h, the transfected cells were plated onto 96-well microtiter plates, which were treated with cell adherent reagent (Applygen) in advance. After another 12 h, cells were treated with Hank's balanced salt solution for starvation and then incubated in CO_2-independent media containing 2% GloSensor cAMP Reagent (Promega) at a volume of 50 μL per well. Then adding varying concentrations of agonist for 5–10 min and measuring luminescence. For G_i-coupled receptors, pre-incubating with varying concentrations of agonist for 10 min. Add 1 μM forskolin (Sigma) to all wells and incubate for 20 min at room temperature before measurements for luminescence. We carried out a nonlinear regression analysis using sigmoidal dose-response in GraphPad Prism to calculate the values of Emax and half-maximum effective concentration (EC_{50}).

Detection of surface expression of mutants

The 5-HT_4, 5-HT_6, and 5-HT_7 mutants were cloned into pcDNA6.0 or pBiT1.1 vector (Invitrogen) with a FLAG tag at its N-terminus. A cell seeding and transfection follow the same method as cAMP accumulation assay. After 24 h of transfection, cells were washed with PBS once and digested with 0.2% (w/v) EDTA in PBS. Cells were blocked with 5% (w/v) BSA (dissolved in PBS) for 15 min at room temperature, and then incubated with primary anti-Flag antibody (dissolved in PBS and containing 5% BSA at a ratio of 1:300, Sigma) for 1 h at room temperature. After that cells were washed 3 times with PBS containing 1% (w/v) BSA before incubating with anti-mouse Alexa-488-conjugated secondary antibody (diluted with PBS containing 5% BSA at a ratio of 1:1000, Invitrogen) at 4°C in the dark for 1 h. After another 3-times wash, resuspended the cells, and fluorescence intensity was quantified in a BD Accuri C6 flow cytometer system (BD Biosciences) at excitation 488 nm and emission 519 nm. Approximately 10,000 cellular events per sample were collected and data were normalized to WT.

Cryo-EM grid preparation and data collection

For the preparation of cryo-EM grids, 3 μL of the purified complexes at concentration 24 mg/mL for the 5-HT-5-HT_4-G_s complex, 35 mg/mL for the 5-HT-5-HT_4-G_i complex, 6 mg/mL for the 5-HT-5-HT_6-G_s complex, and 7 mg/mL for the 5-CT-5-HT_7-G_s complex were applied individually onto a glow-discharged holey carbon grid (Quantifoil R1.2/1.3). Grids were plunge-frozen in liquid ethane using Vitrobot Mark IV (Thermo Fischer Scientific). Frozen grids were transferred to liquid nitrogen and stored for data acquisition. As for the 5-HT-5-HT_4-G_s complex, cryo-EM imaging was performed on a Titan Krios at 300 kV using Gatan K3 Summit detector in the Shuimu BioSciences Ltd. (Beijing, China). The micrographs were recorded using a K3 Summit direct electron detector (Gatan) with a Gatan energy filter (operated with a slit width of 20 eV) (GIF). The images were recorded at a dose rate of about 18.0 $e^-/Å^2/s$ with a defocus ranging from −1.2 to −2.2 μm. The total exposure time was 3.3 s and intermediate frames were recorded in 0.104 s intervals, resulting in a total of 32 frames per micrograph. For the 5-HT-5-HT_4-G_i complex, cryo-EM imaging was performed on a Titan Krios at 300 kV using Gatan K3 Summit detector in the Center of Cryo-Electron Microscopy at Shanghai Institute of Materia Medica, Chinese Academy of Sciences (Shanghai, China). The micrographs were recorded using a K3 Summit direct electron detector (Gatan) with a Gatan energy filter (operated with a slit width of 20 eV) (GIF). The images were recorded at a dose rate of about 26.7 $e^-/Å^2/s$ with a defocus ranging from −1.2 to −2.2 μm using the SerialEM software (Mastronarde, 2005). The total exposure time was 3 s and intermediate frames were recorded in 0.083 s intervals, resulting in a total of 36 frames per micrograph. For the 5-HT-5-HT_6-G_s complex and 5-CT-5-HT_7-G_s complex, cryo-EM imaging were performed on a Titan Krios at 300 kV using Gatan K2 Summit detector in the Center of Cryo-Electron Microscopy, Zhejiang University (Hangzhou, China). Micrographs were recorded in counting mode at a dose rate of about 8.0 $e^-/Å^2/s$ with a defocus ranging from −1.0 to −3.0 μm using the SerialEM software (Mastronarde, 2005). The total exposure time was 8 s and 40 frames were recorded per micrograph.

Image processing and map construction

Dose-fractionated image stacks were aligned using MotionCor2.1 (Zheng et al., 2017). Contrast transfer function (CTF) parameters for each micrograph were estimated by Gctf (Zhang, 2016). Cryo-EM data processing was performed using RELION-3.0-beta2 (Scheres, 2012; Zivanov et al., 2018).

For the 5-HT-5-HT_4-G_s complex, automated particle picking yielded 4,749,375 particles that were subjected to reference-free 2D classification to discard poorly defined particles, producing 1,239,027 particles. This subset of particle projections was subjected to a round of maximum-likelihood-based three-dimensional classification, resulting in two well-defined subsets. The selected subset

was subsequently subjected to 2 rounds of 3D classification. One subset with 359,535 particles shows the complex bound Nb35 and other five subsets with 1,272,036 particles shows the complex not bound Nb35. The Nb35-bound or non-Nb35-bound particles were subsequently subjected to 3D refinement, CTF refinement, Bayesian polishing, and Post-process separately. The final refinement of 5-HT_4-G_s-Nb35 complex generated a map with an indicated global resolution of 3.1 Å, and the final refinement of no Nb35 bound 5-HT_4-G_s-Nb35 complex generated a map with an indicated global resolution of 3.2 Å at a Fourier shell correlation of 0.143.

For the 5-HT-5-HT_4-G_i-scFv16 complex, automated particle picking produced 9,966,637 particles, which were subjected to 2D classification. 1,523,156 particles were selected for 2 rounds of 3D classification. Two subsets with the higher resolution and the better receptor density were selected. The selected subset was subjected to 3D refinement, CTF refinement, and Bayesian polishing. The final refinement generated a map with an indicated global resolution of 3.2 Å at a Fourier shell correlation of 0.143. Although the global resolutions are close, the TMD density of 5-HT_4 in the 5-HT_4-G_i-scFv16 structure is significantly weaker than that in the 5-HT_4-G_s structures. To better model the 5-HT_4-G_i-scFv16 structure, we used DeepEMhancer (Sanchez-Garcia et al., 2021) to generate a sharpen map.

For the 5-HT-5HT_6-Gs-Nb35 complex dataset, auto-picking yielded 5,088,425 particle projections that were subjected to reference-free 2D classification to discard false positive particles or particles categorized in poorly defined classes, producing 1,911,781 particle projections for further processing. This subset of particle projections was subjected to a round of maximum-likelihood-based three-dimensional classification with a pixel size of 2.028 Å. Another round of 3D classification with mask on the complex produced a subset of 153,383 particle projections for the final reconstruction. After the last round of refinement, the final map had an indicated global resolution of 3.3 Å at a Fourier shell correlation (FSC) of 0.143.

For the 5CT-5HT_7-Gs-Nb35 complex dataset, auto-picking yielded 2,174,461 particle projections that were subjected to a round of maximum-likelihood-based three-dimensional classification with a pixel size of 2.028 Å. Another round of 3D classification with mask on the complex produced a subset of 88,238 particle projections for the final reconstruction. After the last round of refinement, the final map had an indicated global resolution of 3.2 Å at a Fourier shell correlation (FSC) of 0.143. Local resolution was determined using the Bsoft (Heymann, 2018) package with half maps as input maps.

Model building and refinement

The crystal structure of human dopamine D3 receptor in complex with eticlopride (PDB code: 6PBL) and the G_i protein model (PDB code: 6PT0) were used as the start for model rebuilding and refinement against the electron microscopy map. The model was docked into the electron microscopy density map using Chimera (Pettersen et al., 2004), followed by iterative manual adjustment and rebuilding in COOT (Emsley and Cowtan, 2004). Real space and reciprocal space refinements were performed using Phenix programs (Adams et al., 2010). The model statistics was validated using MolProbity (Chen et al., 2010). Structural figures were prepared in Chimera and PyMOL (https://PyMOL.org/2/). The final refinement statistics are provided in Table S1.

Selection of representative structures

Including the 4 structures reported here, there are 31 $G_{i/o}$-coupled, 30 G_s-coupled and 3 $G_q/_{11}$-coupled structures. To avoid overrepresentation, we selected only one representative structure for each distinct receptor-G protein complex. The selection criteria were i) protein completeness (percent coverage of full-length sequence); ii) G protein in canonical state (similar to the most commonly found conformation in G protein-GPCR complexes); iii) non-chimeric/engineered G protein; iv) resolution, and v) absence of auxiliary proteins. We also preferred human receptors, when available, over other species. The only receptors without a human receptor structure are the μ-opioid receptor (mouse) and the β_1-adrenoceptor (wild turkey), which have 98% and 80% identity, respectively to the human receptor across all residue positions in segments with a shared secondary structure. The sensory opsin receptor family was excluded our analysis. The PDB accession codes, preferred side chains, experimental method, resolution, sequence coverage, auxiliary proteins and additional information for the set of representative structures can be found in Table S2.

Structure preparation for ligand binding mode analysis

The G_s and $G_{i/o}$-coupled structures of 5-HT_4, and the G_s-coupled structures of 5-HT_6 and 5-HT_7 were imported into Maestro (Schrödinger Release 2020-4, Schrödinger, LLC, New York, NY, 2020). They were prepared using Schrödinger's Protein Preparation Wizard (Sastry et al., 2013) in which the bond orders and charges were assigned with the OPLS3e force field (Roos et al., 2019), hydrogens were added and disulphide bonds created. The protonation states for the ligands serotonin and 5-CT were generated with Epik (Greenwood et al., 2010; Shelley et al., 2007) at pH 7.0 ± 2.0 and the states with the positively charged amine group were selected. The hydrogen bond networks in the receptors were optimized with ProPKA (Olsson et al., 2011; Sondergaard et al., 2011), also at pH 7.0, with automatic optimization of hydroxyl, Asn, Gln and His side chains using ProtAssign in the Protein Preparation Wizard (Sastry et al., 2013). Other optimization parameters were kept in default values and no minimization was performed.

Length and angle analyses

All helical secondary structures were defined by the automatic secondary structure assignment from Multiple Sequence Viewer in BioLuminate (Schrödinger Release 2020-4: BioLuminate, Schrödinger, LLC, New York, NY, 2020). The lengths of TM5 and TM6 were calculated based on the last helical residue at their intracellular ends relative to their most conserved generic residues position (5x50 and 6x50, respectively). Generic residues tables and sequence alignment were retrieved or generated in GPCRdb (Isberg et al., 2014, 2016; Kooistra et al., 2021; Munk et al., 2016). Analysis of sequence identity and similarity showed that 5-HT_{1A} is the closest

analogue to most receptors with G protein coupled structures (average of 33% identity and 52% similarity in the conserved "generic" domains). To reduce the variance by using a common reference, all receptor structures, except CB_1, CB_2, FPR_2, and EP_4 were sequence-based aligned to the backbone of the 7-transmembrane (7TM) helices of 5-HT_{1A} in PyMOL (The PyMOL Molecular Graphics System, Version 2.4 Schrödinger, LLC. New York, NY, 2020), to an average RMSD of 1.18 ± 0.54 Å. CB_1, CB_2, FPR_2, and EP_4, which have low similarity to 5-HT_{1A}, were subjected to a sequence-independent structural superposition of the 7-transmembrane helix backbones. For each aligned class A GPCR-G protein complex, we calculated the insertion angle between the helical portion of the G protein α-subunit C-terminus (in most cases positions H5.3 to H5.23) and the 7TM bundle axis of the 5-HT_{1A} receptor. The 7TM bundle axis was calculated by the sum of the vectors for the extracellular portion of each 7TM helix. The individual helix vectors are calculated by fitting a vector to the C-alphas of a defined stretch of six residues of each transmembrane helix (TM1: 1x31-1x36, TM2: 2x59-2x64, TM3: 3x24-3x29, TM4: 4x56-4x61, TM5: 5x39-5x44, TM6: 6x53-6x58, TM7: 7x33-7x38). For the rotation/tilt angle of the H5 within the receptor core, we used a vector fit to the C-alphas of the 5-HT_{1A} TM3 between residue positions 3x25-3x56 as reference, followed by pairwise differences comparison. The angle calculations were done using a customized version of the INSANE-GPCR (INSertion ANglE of G proteins into GPCRs) python script (Henrik Daver, available at https://doi.org/10.5281/zenodo.4957463). For the displacement and rotation of the whole G_α subunit (N-termini excluded, residues 1-33 in $G_{i/o}$ and 1-40 in G_s), we used the 'Angle between domains' PyMOL script, included in the Psico PyMOL module (PSICO: PyMOL ScrIpt COllection, Thomas Holder and Steffen Schmidt, available at https://github.com/speleo3/PyMOL-psico), again using the 5-HT_{1A}-aligned structures and the G_{i1}-protein coupled to 5-HT_{1A} as reference followed by pairwise difference comparisons.

Receptor-G protein interaction matrices

The GPCR-G protein interface interaction matrices for the G_s- and $G_{i/o}$-coupled serotonergic receptors and for the 28 representative class A receptor were generated and retrieved from the GPCRdb GPCR-G Protein Interface Interactions Tool (Kooistra et al., 2021) (available at https://gpcrdb.org/signprot/matrix/). The interface interactions difference matrices (G_s-$G_{i/o}$), which show the unique or most significant difference in receptor-G protein interactions for each subset (serotonin receptors and class A) of G protein coupled complexes were calculated in Microsoft Excel after scaling and renormalization.

Secondary structure prediction

The aligned sequences for the TM5, ICL3 and TM6 (generic numbers between 5x50 and 6x50) of the 28 class A receptor with G protein coupled structure available were retrieved from GPCRdb (Isberg et al., 2014, 2016; Kooistra et al., 2021; Munk et al., 2016). The gaps were removed and a stretch of 40 residues from 5x50 to 'pseudo-position' 5x89 and from 'pseudo-position' 6x11 to position 6x50 were selected and exported in FASTA format. The secondary structure of these amino acid stretches from the intracellular ends of TM5 and TM6 was predicted using the JPred4 Protein Secondary Structure Prediction Server (Cuff and Barton, 2000; Drozdetskiy et al., 2015), in batch mode. A threshold helicity score of 0.90 was applied to define the number of helical residues in each strech.

Sequence-based identification of G_s vs. $G_{i/o}$ binding determinants and selectivity residue micro-switches

Residue positions were selected based on location in cytosolic TM5 and TM6, being helical (rather than part of the third intracellular loop) in a majority of receptors, and interactions with G proteins in structure complexes with at least two different GPCRs. The analysis of G_s vs. $G_{i/o}$ binding determinants and selectivity residue micro-switches used GPCRdb's sequence signature tool (Kooistra et al., 2021) to conduct a comparative sequence analysis of 33 and 109 receptors activating primarily G_s and $G_{i/o}$, respectively (Hauser et al., 2022). The analysis of residue properties conserved in both G protein families was performed using GPCRdb's sequence alignments (Isberg et al., 2016) for 9 receptors that activate both the G_s and $G_{i/o}$ family with an E_{max}/EC_{50} value differing by at most 100-fold in (Avet et al., 2022). These were the α_{1A}-adrenoceptor, CCK_1, ET_A, GPR65, GPR68, H_1, M_1, MC_3, and MC_4 receptors. None of these receptors were included in the sequence signature analysis which focused on GPCRs activating only one of the G_s and $G_{i/o}$ families.

QUANTIFICATION AND STATISTICAL ANALYSIS

Statistical analysis was performed in OriginPro (OriginPro v.2020, OriginLab Corporation, Northampton, MA, USA) and GraphPad. To verify that the angles, displacements, and helix lengths followed a normal distribution, the Shapiro-Wilk normality test was performed, followed by a Levene's test for equality of variances to assure variance homogeneity. For the normally distributed data, analysis of variance (one-way ANOVA) was applied to compare G_s and $G_{i/o}$-coupled receptors, followed by post-hoc Tukey and Bonferroni mean comparisons' tests. For the length of TM6 and rotation angle of the G_α subunit, which did not follow a normal distribution at a 95% confidence interval, the non-parametric Kruskal-Wallis ANOVA was applied, but the population means remained not significantly different. In all statistical tests, a significance level of 0.05 was applied. The data is reported as mean ± SEM.